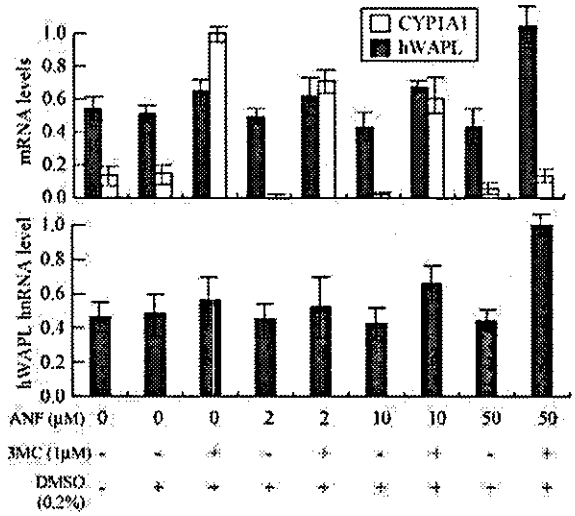

Fig. 5. Effects of AhR inhibition by α-naphthoflavone on *hWAPL* mRNA and hnRNA levels in SiHa cells treated with 3-MC. SiHa cells were treated with 0.2% DMSO alone or 1 μM 3-MC with 0, 2, 10 or 50 μM ANF for 6 h. Then, the *hWAPL* mRNA and hnRNA levels and the *CYP1A1* mRNA levels were deteremined by real time PCR analysis. SiHa cells grown for 6 h in a normal fresh medium without chemicals were also analyzed as a normal control. Data were normalized to the maximaum mRNA and hnRNA levels that were arbitrarily set to 1 in the graphical presentation. *Bars, s.e.*

a well-known target of 3-MC [12,13], we also calculated *CYP1A1* mRNA levels in the three cell lines to confirm the effects of 3-MC on the cells (Fig. 1A). We found that *CYP1A1* mRNA levels in SiHa cells were highest and increased most remarkable. *CYP1A1* mRNA in CaSki cells was not detected in our experiments. We also observed that hWAPL protein level was increased in the 3-MC-treated SiHa cells (Fig. 1B).

We next examined the effects of 3-MC on *hWAPL* expression in SiHa cells at several time points after 3-MC treatment (Fig. 2). The 3-MC-treated cells showed higher levels of *hWAPL* mRNA than the control cells at all time points examined. Interestingly, the *hWAPL* mRNA levels decreased first 6 h and then increased after changing the medium to a fresh medium containing DMSO with or without 3-MC as seen in Fig. 2.

These results prompted us to investigate whether the *hWAPL* expression is related to the cell cycle. First, to synchronize cell cycle progression, we treated SiHa cells with aphidicolin, an inhibitor of DNA synthesis, for 12 h to induce G1-phase arrest. We then released the cells from G1 arrest by changing the culture medium to a fresh growth medium. The synchronized cells were harvested every 4 h for 24 h after release from aphidicolin, and the *hWAPL* mRNA levels were calculated by quantitative real time PCR analysis (Fig. 3A). As seen in Fig. 3A, *hWAPL* mRNA initially decreased and then increased over time. Flow cytometric analysis confirmed the cell cycle phase of the cells at each time point (Fig. 3A). From these results, *hWAPL* mRNA level seemed to fluctuate in accordance with cell cycle profile. However, the levels of *hWAPL* mRNA in the cells treated with nocodazole, an inhibitor of spindle assembly, fluctuated in a similar manner to the aphidicolin-synchronized cells (Fig. 3B). Thus, amounts of *hWAPL* mRNAs are likely to have no relation to the cell cycle profiles. Recently, Guigal et al. demonstrated that FBS induces transcription of the *CYP1A1* gene. Therefore, we suspected that the fluctuation of *hWAPL* mRNA levels might be associated with the culture medium change.

To investigate the effects of components in FBS on the fluctuation of *hWAPL* mRNA levels, we examined the *hWAPL* mRNA levels in SiHa cells after changing growth medium to a fresh medium supplemented with charcoal/dextran treated FBS (CTF) or BSA instead of FBS. The fluctuations of the *hWAPL* mRNA levels showed similar trends among the cells grown with FBS, CTF and BSA (Fig. 4A; left panel). However, all cells examined in Figs. 1–3 were grown in the medium containing DMSO. Thus, we also tested the effects of DMSO with FBS, CTF or BSA at the same time. Interestingly, fluctuations of the *hWAPL* mRNA levels in SiHa cells treated with 0.1% DMSO showed different trends among FBS, CTF and BSA (Fig. 4A; right panel), and the *hWAPL* mRNA levels in the DMSO-treated cells fluctuated more drastically than that in the cells grown without DMSO (Fig. 4B). Especially, remarkable decrease of *hWAPL* mRNA levels for first 6 h after the medium change was distinctive for the growth medium supplemented with FBS and DMSO. These results suggest that DMSO and some constituents of FBS affect *hWAPL* mRNA accumulation synergistically.

mRNA levels do not always reflect on the transcription activity of genes. To investigate the kinetics of the promoter activities of the *hWAPL* gene in the cells, we evaluated the levels of *hWAPL* heterogeneous nuclear RNA (hnRNA), the unprocessed precursor of the mature and functional mRNA.

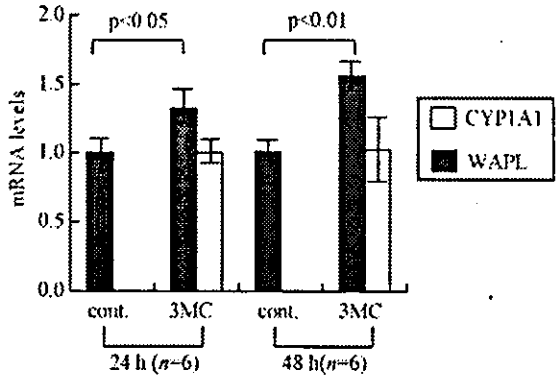

Fig. 6. Effects of 3-MC on *WAPL* mRNA levels in mouse uteri. The mice received a single intraperitoneal injection of 1 ml of olive oil containing 3-MC (3-MC) or olive oil only (cont.), and *WAPL* mRNA levels in the uteri at 24 and 48 h after injection were determined with quantitative real time PCR analysis. *CYP1A1* mRNA levels were also determined to confirm the effects of 3-MC on mouse uteri. The data represent the means of multiple samples normalized to the mean values of the *hWAPL* mRNA levels in the cont. 24 h samples and *CYP1A1* mRNA levels in the 3-MC 24 h samples, respectively, that were arbitrarily set to 1 in the graphical presentation. *Bars, s.e.*

by real time PCR using intron-specific primers for *hWAPL* searched in Ensembl Genome Browser (http://www.ensembl.org/). Levels of hnRNA have been proposed as a surrogate for nuclear run-on assays to determine gene transcription rates [14,15]. Although the *hWAPL* hnRNA levels fluctuated in somewhat different manner to the mRNA levels in the cells grown without DMSO, the *hWAPL* hnRNA levels in the DMSO-treated cells fluctuated in similar manner to the mRNA levels (Fig. 4C; compare with Fig. 4A). These results suggest that DMSO and some components of FBS affect transcriptional activity of the *hWAPL* gene. Increase of *hWAPL* transcription levels at 24 h in common with the cells under various conditions may be caused by the accumulation of wastes in their growth medium.

3-MC is known to be an agonist of AhR [16]. Thus, to investigate whether AhR is related to *hWAPL* transcription activation, we examined the effects of α-naphthoflavone (ANF), an AhR antagonist [17], at a dose of 2, 10 and 50 μM on *hWAPL* mRNA and hnRNA levels in 3-MC-treated SiHa cells by quantitative real time PCR analysis (Fig. 5). We also evaluated *CYP1A1* mRNA levels for monitoring the inhibitory effects on AhR functions by ANF, and found that 50 μM of ANF strongly inhibited AhR functions (Fig. 5; upper panel). Interestingly, increase of *hWAPL* mRNA levels by 3-MC was more remarkable in AhR-inhibited cells rather than that in AhR-functioning normal cells. Induction of *hWAPL* hnRNA levels showed similar manner to the *hWAPL* mRNA (Fig. 5; lower panel). From these results, we hypothesized that AhR was involved in the transcriptional regulation of *hWAPL*, but there are complex mechanisms for the transcriptional regulation of *hWAPL*. We did not find XRE motif in 5000 bp of 5′-upstream sequence of the *hWAPL* gene using MOTIF Sequence Motif Search (http://motif.genome.jp/) at the cut off score 85. Thus, although further investigation is required, we suppose that *hWAPL* is not a direct target of 3-MC but a down stream molecule of a 3-MC-targeted molecule.

Finally, we examined whether the mRNA level of a mouse homolog of *hWAPL* is increased by 3-MC in mouse uterus. Twenty-four and 48 h after the injection of 3-MC into the abdominal cavities of C57/BL6 female mice, we harvested the uteri and analyzed the *WAPL* mRNA levels by quantitative real time PCR analysis. The *CYP1A1* mRNA levels were also analyzed to confirm the 3-MC effects on the uteri. The uteri exhibited increases in *WAPL* mRNA levels compared with that of control mice (Fig. 6). These data suggest that 3-MC exposure affects *WAPL* expression in uterus.

Our recent data demonstrated that the unscheduled increase of *hWAPL* expression in human uterine cervix is associated with cervical cancer [1]. In Addition, previous studies demonstrated that 3-MC induces carcinogenesis in mouse uterine cervix [18, 19]. Thus, although the *hWAPL* induction by 3-MC was weak in our experiments, our results suggest that the promotion of carcinogenesis by 3-MC in uterus is likely to involve the *hWAPL* oncogene.

Acknowledgements

This work was supported by a Grant-in-Aid for scientific research on Priority Area (C) from the Ministry of Education, Science, Sports and Culture, and a grant from Core Research for Evolutional Science and Technology (CREST), Japan Science and Technology Corporation.

References

[1] K. Oikawa, T. Ohbayashi, T. Kiyono, H. Nishi, K. Isaka, A. Umezawa, et al., Expression of a novel human gene, human wings apart-like (hWAPL), is associated with cervical carcinogenesis and tumor progression, Cancer Res. 64 (2004) 3545–3549.

[2] F. Verni, R. Gandhi, M.L. Goldberg, M. Gatti, Genetic and molecular analysis of wings apart-like (wapl), a gene controlling heterochromatin organization in *Drosophila melanogaster*, Genetics 154 (2000) 1693–1710.

[3] K.W. Dobie, C.D. Kennedy, V.M. Velasco, T.L. McGrath, J. Weko, R.W. Patterson, G.H. Karpen, Identification of chromosome inheritance modifiers in *Drosophila melanogaster*, Genetics 157 (2001) 1623–1637.

[4] S. Reynaud, C. Duchiron, P. Deschaux, 3-Methylcholanthrene increases phorbol 12-myristate 13-acetate-induced respiratory burst activity and intracellular calcium levels in common carp (Cyprinus carpio L.) macrophages, Toxicol. Appl. Pharmacol. 175 (2001) 1–9.

[5] J. Mimura, Y. Fujii-Kuriyama, Functional role of AhR in the expression of toxic effects by TCDD, Biochim. Biophys. Acta 1619 (2003) 263–268.

[6] K. Sogawa, Y. Fujii-Kuriyama, Ah receptor, a novel ligand-activated transcription factor, J. Biochem. (Tokyo) 122 (1997) 1075–1079.

[7] K. Oikawa, T. Ohbayashi, J. Mimura, R. Iwata, A. Kameta, K. Evine, et al., Dioxin suppresses the checkpoint protein, MAD2, by an aryl hydrocarbon receptor-independent pathway, Cancer Res. 61 (2001) 5707–5709.

[8] S.R. Kondraganti, P. Fernandez-Saluguero, F.J. Gonzalez, K.S. Ramos, W. Jiang, B. Moorthy, Polycyclic aromatic hydrocarbon-inducible DNA adducts: evidence by 32P-postlabeling and use of knockout mice for Ah receptor-independent mechanisms of metabolic activation in vivo, Int. J. Cancer 103 (2003) 5–11.

[9] K. Oikawa, T. Ohbayashi, J. Mimura, Y. Fujii-Kuriyama, S. Teshima, K. Rokutan, et al., Dioxin stimulates synthesis and secretion of IgE-dependent histamine-releasing factor, Biochem. Biophys. Res. Commun. 290 (2002) 984–987.

[10] M. Kuroda, T. Ishida, M. Takanashi, M. Satoh, R. Machinami, T. Watanabe, Oncogenic transformation and inhibition of adipocytic conversion of preadipocytes by TLS/FUS-CHOP type II chimeric protein, Am. J. Pathol. 151 (1997) 735–744.

[11] K. Oikawa, Y. Kosugi, T. Ohbayashi, A. Kameta, K. Isaka, M. Takayama, et al., Increased expression of IgE-dependent histamine-releasing factor in endometriotic implants, J. Pathol. 199 (2003) 318–323.

[12] N. Guigal, E. Seree, V. Bourgarel-Rey, Y. Barra, Induction of CYP1A1 by serum independent of AhR pathway, Biochem. Biophys. Res. Commun. 267 (2000) 572–576.

[13] N. Guigal, E. Seree, Q.B. Nguyen, B. Charvet, A. Desobry, Y. Barra, Serum induces a transcriptional activation of CYP1A1 gene in HepG2 independently of the AhR pathway, Life Sci. 68 (2001) 2141–2150.

[14] C.J. Elferink, J.J. Reiners Jr., Quantitative RT-PCR on CYP1A1 heterogeneous nuclear RNA: a surrogate for the in vitro transcription run-on assay, Biotechniques 20 (1996) 470–477.

[15] R.F. Johnson, C.M. Mitchell, W.B. Giles, W.A. Walters, T. Zakar, The in vivo control of prostaglandin H synthase-2 messenger ribonucleic acid expression in the human amnion at parturition, J. Clin. Endocrinol. Metab. 87 (2002) 2816–2823.

[16] M. Naruse, Y. Ishihara, S. Miyagawa-Tomita, A. Koyama, H. Hagiwara, 3-Methylcholanthrene, which binds to the arylhydrocarbon receptor, inhibits proliferation and differentiation of osteoblasts in vitro and ossification in vivo, Endocrinology 143 (2002) 3575–3581.

[17] T.A. Gasiewicz, G. Rucci, Alpha-naphthoflavone acts as an antagonist of 2,3,7, 8-tetrachlorodibenzo-p-dioxin by forming an inactive complex with the Ah receptor, Mol. Pharmacol. 40 (1991) 607–612.

[18] P. Das, A.R. Rao, P.N. Srivastava, Influence of ascorbic acid on MCA-induced carcinogenesis in the uterine cervix of mice, Cancer Lett. 72 (1993) 121–125.

[19] S. Gagandeep, S. Dhanalakshmi, E. Mendiz, A.R. Rao, R.K. Kale, Chemopreventive effects of Cuminum cyminum in chemically induced forestomach and uterine cervix tumors in murine model systems, Nutr. Cancer 47 (2003) 171–180.

Molecular Biology of the Cell
Vol. 16, 1491–1499, March 2005

Immortalization of Human Fetal Cells: The Life Span of Umbilical Cord Blood-derived Cells Can Be Prolonged without Manipulating p16^{INK4a}/RB Braking Pathway[D]

Masanori Terai,*† Taro Uyama,* Tadashi Sugiki,* Xiao-Kang Li,‡ Akihiro Umezawa,*§ and Tohru Kiyono†

Departments of *Reproductive Biology and Pathology and ‡Innovative Surgery, National Research Institute for Child Health and Development, Tokyo 157-8535, Japan; †Virology Division, National Cancer Center Research Institute, Tokyo, Japan; and §Department of Pathology, Keio University School of Medicine, Tokyo 160-8582, Japan

Submitted July 31, 2004; Accepted December 20, 2004
Monitoring Editor: Lawrence Goldstein

Human umbilical cord blood-derived mesenchymal stem cells (UCBMSCs) are expected to serve as an excellent alternative to bone marrow-derived human mesenchymal stem cells. However, it is difficult to study them because of their limited life span. To overcome this problem, we attempted to produce a strain of UCBMSCs with a long life span and to investigate whether the strain could maintain phenotypes in vitro. UCBMSCs were infected with retrovirus carrying the human telomerase reverse transcriptase (hTERT) to prolong their life span. The UCBMSCs underwent 30 population doublings (PDs) and stopped dividing at PD 37. The UCBMSCs newly established with hTERT (UCBTERTs) proliferated for >120 PDs. The p16^{INK4a}/RB braking pathway leading to senescence can be inhibited by introduction of Bmi-1, a polycomb-group gene, and human papillomavirus type 16 E7, but the extension of the life span of the UCBMSCs with hTERT did not require inhibition of the p16^{INK4a}/RB pathway. The characteristics of the UCBTERTs remained unchanged during the prolongation of life span. UCBTERTs provide a powerful model for further study of cellular senescence and for future application to cell-based therapy by using umbilical cord blood cells.

INTRODUCTION

Human mesenchymal stem cells (hMSCs) can be a useful source of cells for transplantation for several reasons: they have the ability to proliferate and differentiate into mesodermal tissues, and they entail no ethical or immunological problems (Caplan, 1991; Prockop, 1997; Caplan and Bruder, 2001). hMSCs have been studied extensively over the past 3 decades, and numerous independent research groups have successfully isolated hMSCs from a variety of sources, most commonly, from the bone marrow (Owen, 1988; Umezawa *et al.*, 1992; Jaiswal *et al.*, 1997; Makino *et al.*, 1999; Pittenger *et al.*, 1999; Sekiya *et al.*, 2004). Umbilical cord blood (UCB) contains circulating stem/progenitor cells, and the cells contained in UCB are known to be distinct from those contained in bone marrow and adult peripheral blood (Mayani and Lansdorp, 1998). Isolation, characterization, and differentiation of clonally expanded hMSCs derived from UCB (UCBMSCs) have been reported (Goodwin *et al.*, 2001; Lee *et al.*, 2004), and UCBMSCs have been found to have multipotency, and the immunophenotype of the clonally expanded cells is consistent with that reported for bone marrow mesenchymal stem cells. Even now, most UCB is regarded as medical waste in the delivery rooms. Aspirating bone marrow from patients is, however, an invasive procedure, and the proliferation and differentiation capacity of hMSCs decreases with the donor age (D'Ippolito *et al.*, 1999). Therefore, the applications of UCB should be further expanded.

UCBMSCs will be useful sources for cell transplantation, however, it is difficult to study and apply them because of their limited life span. One of the reasons for this is that normal human cells undergo a limited number of cell division in culture and then enter a nondividing state called "senescence" (Hayflick, 1976; Campisi, 1997). Human cells reach senescence or cease to divide after a limited number of cell replications, and the average number of hMSC population doublings (PDs) has been found to be ~40 (Takeda *et al.*, 2004), implying that it would be difficult to obtain enough cells to restore the function of a failing human organ. Large numbers of cells must be injected into damaged tissues to restore function in humans, and cells sometimes need to be injected throughout entire organs.

To resolve these problems, the life span of hMSCs from bone marrow can be extended by retroviral transduction of human telomerase reverse transcriptase (hTERT) (Blackburn, 2000a,b, 2001) and human papillomavirus type 16 (HPV16) E6 and/or E7 (Sekiguchi *et al.*, 1999; Burk *et al.*, 2003; Takeda *et al.*, 2004). Both p16^{INK4a}/RB inactivation with E7 and telomerase activation with E6 are required to extend the life span of human mammary epithelial cells (Kiyono *et al.*, 1998). E6 also accelerates degradation of p53, which induces the cdk inhibitor p21 (Sekiguchi and Hunter, 1998). This system in which p16^{INK4a}/RB is inhibited and

This article was published online ahead of print in *MBC in Press* (http://www.molbiolcell.org/cgi/doi/10.1091/mbc.E04–07–0652) on January 12, 2005.

[D] The online version of this article contains supplemental material at *MBC Online* (http://www.molbiolcell.org).

Address correspondence to: Akihiro Umezawa (umezawa@1985.jukuin.keio.ac.jp).

telomerase is activated is highly efficient in extending the life span of hMSCs (Okamoto *et al.*, 2002).

In the present study, we investigated the growth regulatory mechanism of UCBMSCs and attempted to establish UCBMSCs with hTERT (UCBTERTs) to overcome their limited life span. Introduction of hTERT alone was sufficient to extend the life span of UCBMSCs in vitro, and this technique for prolonging the life span of UCBMSCs will be a useful tool. UCBTERTs with the extended life span provide a powerful model for further study of cellular senescence and application to transplantation therapy in the future.

MATERIALS AND METHODS

Isolation and Cell Culture of UCBMSCs

UCB was collected on delivery with informed consent. UCB mononuclear cells were obtained as per the manufacturer's instructions, followed by Ficoll-Paque (Amersham Biosciences, Piscataway, NJ) density gradient centrifugation (1.077 g/cm^3), and plated in tissue culture dishes (BD Biosciences, San Jose, CA) in DMEM medium (Sigma-Aldrich, St. Louis, MO) and 10% fetal bovine serum (FBS) (Vitromex, Geilenkirchen, Germany). All cultures were maintained at 37°C in a humidified atmosphere containing 95% air and 5% CO_2. A few colonies were found in the culture dish 1 mo after the collected cells were cultured in DMEM with 10% FBS. One colony was trypsinized using a colony cylinder and then diluted and plated on 12-well plates (BD Biosciences) in mesenchymal stem cell growth medium (MSCGM, PT-3001; Cambrex Bio Science Walkersville, Walkersville, MD) at a final density of ~4 × 10^5 cells/well in a 12-well plate. MSCGM was used in all culture procedures after harvesting the colony. The cells were passaged at a density of ~1 × 10^5 cells/100-mm dish (1:4), and the original cells were regarded as being PD 0 (day 0). When the cultures reached subconfluence, the cells were harvested with 0.25% trypsin and 1 mM EDTA and replated with one-half of the harvested cells. Cells were allowed to adhere overnight, and nonadherent cells were washed out with medium changes. Medium changes were carried out twice weekly thereafter. The cells were cultured for further experiments under the approval (approval nos. 7 and 55) of the Ethics Committee of National Research Institute for Child Health and Development, Tokyo.

Infection with Recombinant Retroviruses

The cells were prepared for infection with recombinant retroviruses expressing the E6, E7, and hTERT, as described previously (Takeda *et al.*, 2004). Stably transduced cells with an expanded life span were designated UCBE6E7-20 and UCBTERT-21 cells.

Senescence-associated-β-gal (SA-β-gal) Staining

The SA-β-gal assay was performed as described previously (Dimri *et al.*, 1995). Cells were washed in phosphate-buffered saline (PBS), fixed for 3–5 min at room temperature in 2% formaldehyde/0.2% glutaraldehyde (or 3% formaldehyde), washed, and incubated at 37°C with fresh SA-β-gal stain solution: 1 mg of 5-bromo-4-chloro-3-indolyl β-D-galactosidase per milliliter (stock is 20 mg of dimethylformamide/ml), 40 mM citric acid/sodium phosphate, pH 6.0, 5 mM potassium ferrocyanide, 5 mM potassium ferricyanide, 150 mM NaCl, and 2 mM $MgCl_2$. Staining was evident in 2–4 h and maximal in 12–16 h.

Cell Transplantation

Freshly collected confluent cells (10^6 cells) were subcutaneously and intramuscularly injected into BALB/c nu/nu mice (Sankyo Laboratory, Hamamatsu, Japan). Animals were monitored for malignant transformation of the injected cells for 3 mo after inoculation and then killed by cervical location.

Flow Cytometric Analysis

Cells were stained for 30 min at 4°C with primary antibodies and immunofluorescent secondary antibodies. The cells were then analyzed on a FACScan (BD Biosciences), and the data were analyzed with the CELLQUEST software (BD Biosciences). Antibodies against human CD13, CD14, CD29, CD31, CD34, CD44, CD45, CD50, CD55, CD59, CD90, CD117, and CD133 were purchased from Beckman Coulter (Fullerton, CA), Immunotech (Marseille, France), Cytotech (Hellebaek, Denmark), and BD Biosciences PharMingen (San Diego, CA).

Western Blot Analysis

Cells were seeded at a density of 3 × 10^5 cells/100-mm culture dish and harvested at subconfluence. Cell lysates were prepared by sonication by using ultrasonic homogenizer VP-5S in WE16th lysis buffer (Gewin *et al.*, 2004). Equal amounts of protein (20 μg) were loaded on SDS-polyacrylamide gels and blotted on Immobilon-P membranes (Millipore, Bedford, MA) by using a semidry transfer system (Atto, Tokyo, Japan). The primary antibodies used were as follows: G3-245 for retinoblastoma (RB) protein and G175-405 for p16^{INK4a} (BD Biosciences PharMingen), DO-1 for p53 (Oncogene Science, Cambridge, MA), F-5 for p21 and I-19 for actin (Santa Cruz Biotechnology, Santa Cruz, CA), affinity-purified anti-phospho-ataxia telangiectasia mutated kinase (p-ATM) (Ser1981) (600-401-400; Rockland, Gilbertsville, PA), and phospho-p53 (p-p53) (Ser15) antibody (9284; Cell Signaling Technology, Beverly, MA). Blots were probed with horseradish peroxidase-conjugated goat anti-mouse IgG (Jackson ImmunoResearch Laboratories, West Grove, PA), anti-rabbit IgG (New England Biolabs, Beverly, MA), or donkey anti-goat IgG (Santa Cruz Biotechnology), and visualized using an enhanced chemiluminescence detection kit (Roche Diagnostics, Indianapolis, IN).

Telomere Length Assay

Total genomic DNA was isolated from cultured cells by proteinase K digestion. The lengths of telomere in each sample were determined by Southern blot analysis as described previously (Vaziri *et al.*, 1994). Briefly, 1 μg of genomic DNA extracted from each sample was digested with both *Hinf*I and *Rsa*I and electrophoresed in 0.8% agarose gels for 16 h, transferred onto a Hybond N membrane (Amersham Biosciences), and hybridized with digoxigenin (DIG)-labeled $(TTAGGG)_3$ probe. The membrane was incubated with anti-DIG alkaline phosphatase (ALP) antibody, and detection was performed with chemiluminescence solution.

Telomerase Activity

Telomerase activity in each sample was detected by the telomeric repeat amplification protocol (TRAP) assay by using the TRAPeze kit (Intergen, Purchase, NY) according to the manufacturer's instruction.

Karyotype Analysis

Fixation and chromosome preparation were performed according to the standard procedure described previously (Sasaki, 1975). For each sample, >50 cells were scored for their chromosome number.

Differentiation-Induction Experiments

The multidirectional differentiation potential of each cell line was assessed by the differentiation-induction protocols described below.

Histochemical Staining

After 21 d of culture, cells were rinsed twice with PBS and then fixed with 10% buffered formalin for 10 min at room temperature. The fixed cells were stained with 0.3% Oil-Red-O (Nakarai Tesque, Kyoto, Japan) for the adipogenic differentiation assay and with 5% silver nitrate (Nakarai Tesque) for von Kossa staining in the osteogenic differentiation assay (Tsuchiya *et al.*, 2004).

Osteogenic Differentiation

Cells were seeded at a density of 5 × 10^4 cells/cm^2 in tissue culture dishes and cultured with MSCGM containing 100 nM dexamethasone, 50 μM ascorbic, acid 2-phosphate, and β-glycerophosphate. The cultures were maintained for 4 wk, and the cultured medium was replaced every 3 d.

Adipogenic Differentiation

Cells were seeded at a density of 3 × 10^4 cells/cm^2 in tissue culture dishes. When the cells were confluent, the adipogenic differentiation was initiated by three cycles of induction/maintenance culture. Each cycle consists of 3 d of culture in the induction medium (DMEM with 10% FBS, 1 μM dexamethasone, 0.2 mM indomethacin, 10 μg/ml insulin, and 0.5 mM 3-isobutyl-1-methylxanthine) followed by 2 d of culture in the maintenance medium (DMEM with 10% FBS and 10 μg/ml insulin).

RESULTS

Establishment of UCB-derived Cells with an Extended Life Span

UCBMSCs regarded as being PD 0, or day 0, were fibroblast-like in morphology, indistinguishable in appearance from the marrow-derived MSCs, and relatively larger in size than rapidly self-renewing stem cells (Prockop *et al.*, 2001) and multipotent adult progenitor stem cells (Jiang *et al.*, 2002) (Figure 1A). The cells from PD 9 to PD 31 rapidly proliferated in culture, and propagated continuously (Figure 1, B and C). No SA-β-gal activity was detected histoenzymologically in the UCBMSCs in the growth phase on day 59. The UCBMSCs stopped replicating, became broad and flat, and exhibited SA-β-gal activity as indicated by blue staining of

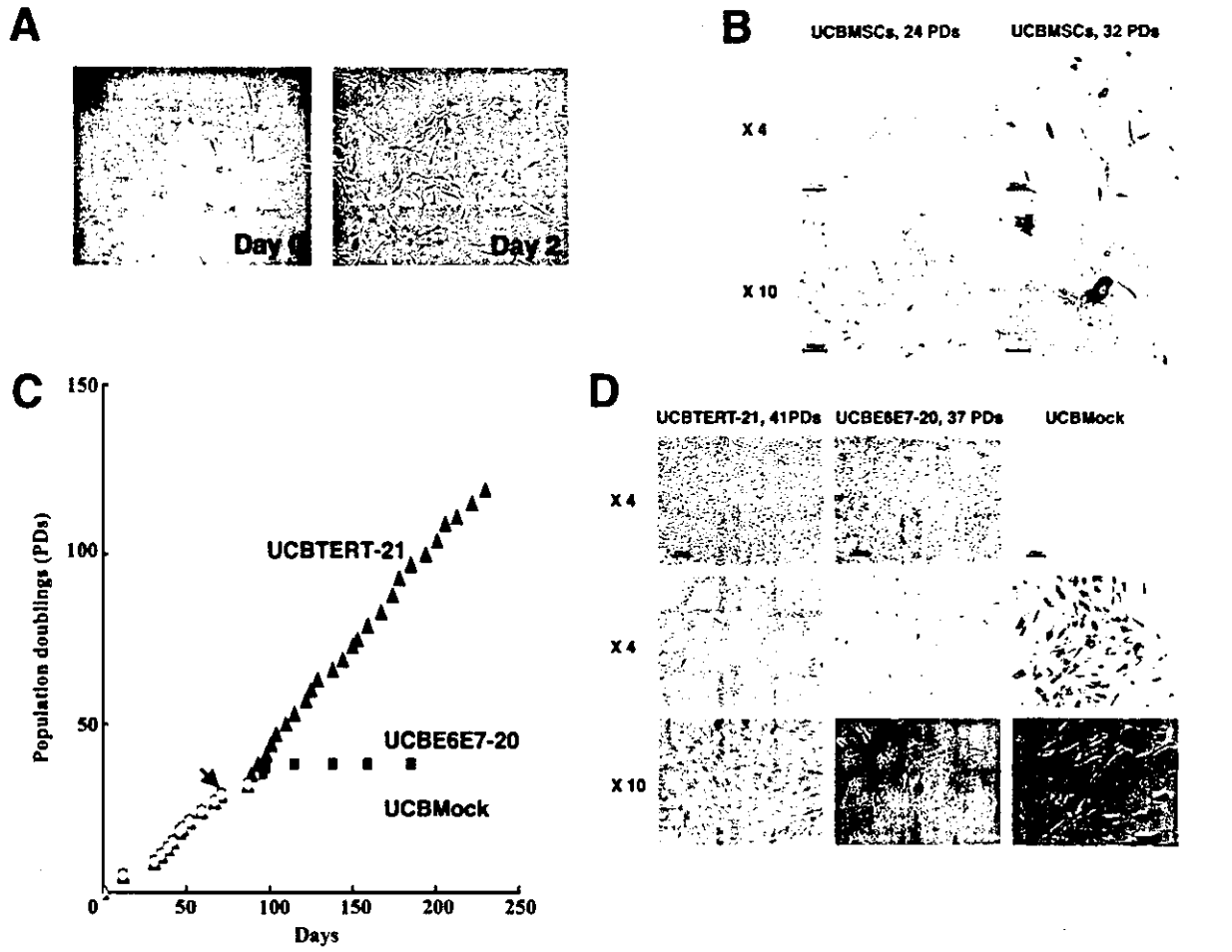

Figure 1. In vitro growth and SA-β-gal activity of UCBMSCs, UCBE6E7-20 cells, and UCBTERT-21 cells. (A) Morphology of human UCBMSCs (left, day 0; right, day 2; original magnification, 10×). (B) Morphological changes and SA-β-gal activity of UCBMSCs. UCBMSCs were a broad and flat, ceased to proliferate, and exhibited high SA-β-gal activity as indicated by their cytoplasm staining blue at PD 32 (14 passages at day 98), suggesting senescence. No SA-β-gal activity was detected in the UCBMSCs in the growth phase at PD 24 (10 passages at day 59 in left column). Bar, 250 μm in the upper column and 100 μm in the lower column. (C) Population doublings of UCBMock cells (yellow circles), UCBE6E7-20 cells (red squares), and UCBTERT-21 cells (blue triangles) are shown. UCBMSCs were infected with recombinant retroviruses carrying E6 and E7 or hTERT or were treated with polybrene alone at PD 29 (indicated as an arrow). UCBTERT-21 cells proliferated for >120 PDs and for >250 d and exhibited persistent growth. UCBE6E7-20 cells exhibited a prolonged cell life span in culture, reached 38 PDs, and then entered crisis. UCBMock cells stopped growing and entered senescence at 32 PDs. (D) Morphological changes (top column) and SA-β-gal activity (middle and bottom column) of UCBMock cells, UCBE6E7-20 cells, and UCBTERT-21 cells. No staining was detected in UCBTERT-21 cells at PD 41 (left column, 16 passages at day 98) with the SA-β-gal stain (middle and bottom columns). A few UCBE6E7 cells were positive with SA-β-gal stain at PD 37 (middle column, 15 passages at day 98). UCBMock cells were broad and flat at PD 32 (right column, 14 passage at day 98), indicating senescence.

their cytoplasm at PD 32 or day 98, indicating that they had entered senescence (Figure 1, B and C). The morphological changes and SA-β-gal activity of UCBMSCs are PD dependent. To extend the cells' life span and obtain a large number of cells, two different types of cells were obtained by transferring a combination of HPV16 E6 and E7 or hTERT at 29 PDs or 12 passages (Figure 1C, indicated as an arrow). UCBMSCs transduced with a combination of E6 and E7 were designated UCBE6E7-20 cells, and UCBMSCs transduced with hTERT were named UCBTERT-21 cells. UCBTERT-21 cells successfully proliferated >120 PDs, and continued to grow. The cells were found to have an extended life span (Figure 1C, UCBTERT-21 cells, blue triangles). The UCBE6E7-20 cells, which had been transduced with E6 and E7, had a prolonged cell life span in culture, and underwent global cell death at 38 PDs, when the cells entered a "crisis" period. This implies that the E6 and E7 are capable of prolonging cell life span but that their effect is limited (Figure 1C, UCBE6E7-20 cells, pink squares). Mock infection (polybrene treatment alone) did not extend cell life span, and the cells reached senescence or cessation of growth at PD 32 (Figure 1C, UCBMock, yellow circles). SA-β-gal staining was performed to determine the proportions of cells that had entered senescence, and positive staining was observed in 0% of the UCBTERT-21 cells at PD 41, 2% of the UCBE6E7-20 cells at PD 37, and 100% of the UCBMock cells at PD 32 (Figure 1D). The low percentage of SA-β-gal–positive UCBE6E7-20 cells at PD 37 or day 98 is probably attributable to global cell death by crisis (Figure 1D, middle column). UCBMock cells exhibited a typical senescence-associated morphology, i.e., they were broad and flat and exhibited strong SA-β-

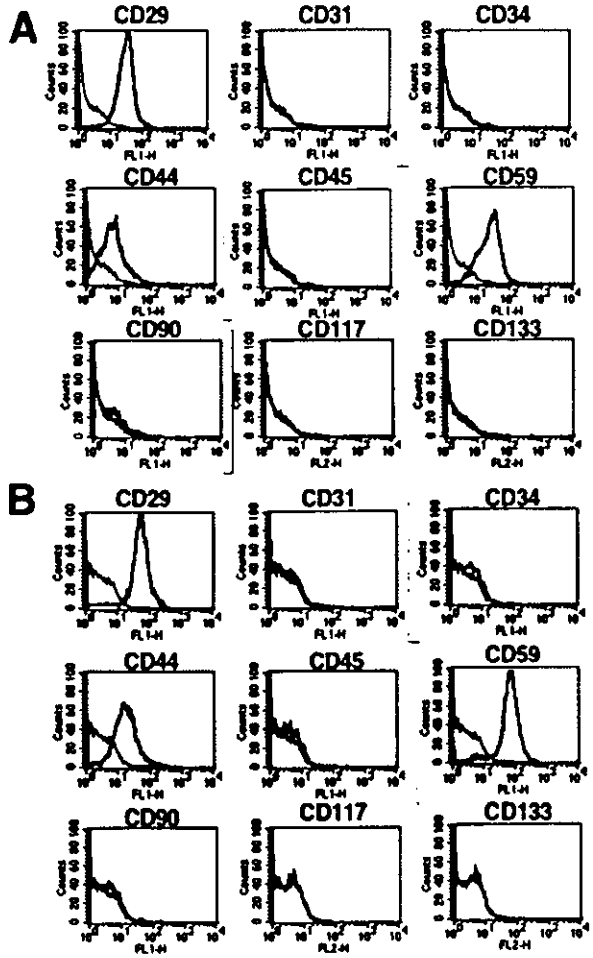

C

Surface marker	UCBMSCs	UCBTERT-21
CD34	-	-
CD117	-	-
CD31	-	-
CD13	-	-
CD14	-	-
CD29	+++	+++
CD44	++	++
CD45	-	-
CD50	-	-
CD55	++	++
CD59	+++	+++
CD90	-	-
CD133	-	-

Figure 2. Flow cytometric analysis of cell surface markers of UCBMSCs and UCBTERT-21 cells. UCBMSCs (A) displayed the same pattern of surface markers as UCBTERT-21 cells (B). No difference in cell surface markers was found between UCBMSCs and UCBTERT-21 cells as summarized in the table (C). Both were positive for CD29 (integrin β1), CD44 (Pgp-1/ly-24), and CD59, and negative for CD31 (PECAM-1), CD34, CD45 (leukocyte common antigen), CD90 (Thy-1), CD117 (c-kit), and CD133.

gal activity enzyme cytochemically at PD 32 (Figure 1D, right column).

The cells did not undergo malignant transformation. They stopped dividing after reaching confluence, and they did not form any foci after confluence in vitro. Nor did the cells grafted into the subcutaneous and muscle tissue of nude mice (n = 6) produce tumors, at least during the monitoring period (>100 d). Injected UCBTERT-21 cells survived but did not proliferate at the injection sites.

Unchanged Surface Markers of UCBMSCs after Prolongation of Their Life Span

Expression of UCBMSCs and UCBTERT-21 cell surface markers was evaluated by flow cytometric analysis (Figure 2). The results showed that both cells were positive for CD29 (integrin β1), CD44 (Pgp-1/ly-24), CD55, and CD59, and negative for CD13, CD14 (a marker for macrophages and dendritic cells), CD31 (platelet-endothelial cell adhesion molecule-1, PECAM-1), CD34, CD45 (leukocyte common antigen), CD50 (intercellular adhesion molecule-1, ICAM-1), CD90 (Thy-1), CD117 (c-kit), and CD133. Primary UCBMSCs displayed the same pattern of surface markers as UCBTERT-21 cells, implying that the surface marker expression was unaffected by the exogenously expressed hTERT.

Absence of $p16^{INK4a}$ in Parental UCBMSCs

Expression of $p16^{INK4a}$/RB premature senescence-associated proteins (Figure 3A) and telomere/p53 replicative senescence-associated proteins (Figure 3B) was analyzed in UCBMSCs, UCBTERT-21, and UCBE6E7-20 cells. $p16^{INK4a}$ was not detected in the UCBMSC lanes until the senescence stage; $p16^{INK4a}$ was not detected until PD 53 and started to be expressed in UCBTERT-21 cells at a low level at PD 69, and $p16^{INK4a}$ was detected in UCBE6E7-20 cells at PD 37, immediately before the crisis stage. The protein levels of p53 and p21 in UCBMSCs became up-regulated as the number of PDs increased, but the protein levels of p53 and p21 became down-regulated in UCBE6E7-20 cells, implying that exogenously introduced E6 targets p53 for proteolytic degradation. ATM in UCBE6E7-20 cells was phosphorylated, probably because of DNA damage or telomere length shortening (Figure 3B, lane 8). p53, phosphorylated p53, and p21 were induced by H_2O_2, a physiological stressor, in UCBTERT-21 cells (Figure 3B, lane 9). The hypophosphorylated forms of

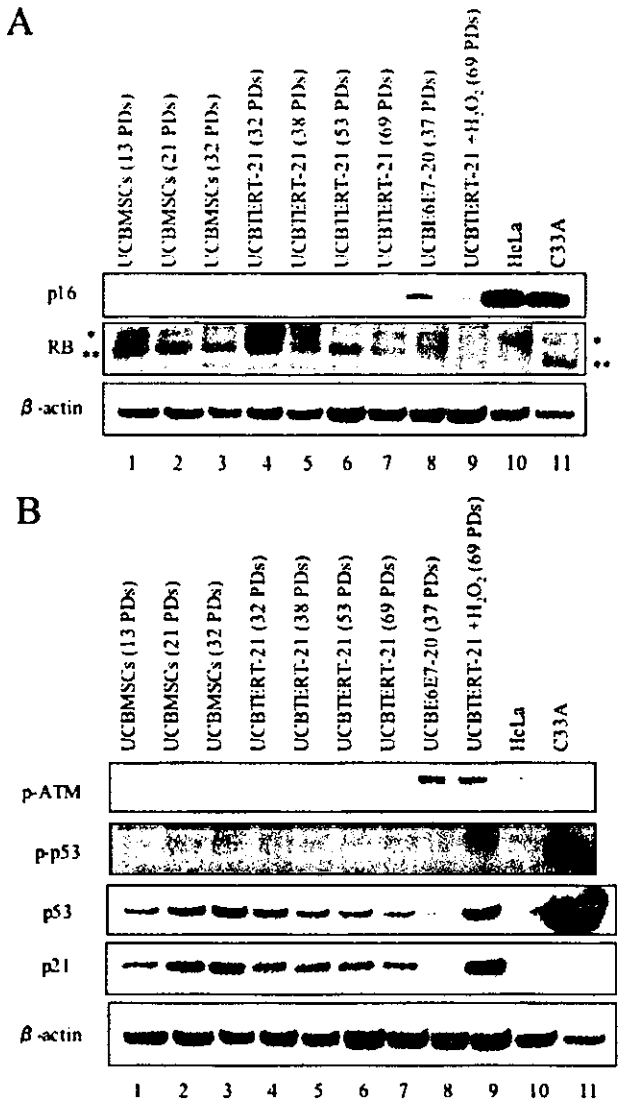

Figure 3. Time-course analysis of cell cycle-associated protein levels in UCBMSCs, UCBE6E7-20 cells, and UCBTERT-21 cells. UCBMSCs, UCBE6E7-20 cells, and UCBTERT-21 cells were analyzed by Western blotting for cell cycle-associated $p16^{INK4a}$, RB, p-ATM (Ser1981), phospho-p53 (p-p53) (Ser15), p53, p21 and β-actin protein levels. (A) "$p16^{INK4a}$-RB" senescence (premature senescence) pathway-associated protein levels, i.e., $p16^{INK4a}$ and RB. The hyperphosphorylated and hypophosphorylated forms of RB were indicated as a single asterisk and double asterisks, respectively. (B) Telomere shorten-p53' senescence (replicative senescence) pathway-associated protein levels, i.e., p-ATM, p-p53, p53, and p21. Cells were cultured for the PDs indicated and assayed. Expression of β-actin protein was monitored as a loading control.

RB became dominant and the hyperphosphorylated forms decreased with passage of UCBMSCs (Figure 3A, lanes 1–3), correlating to the increase in p53 and p21 (Figure 3B, lanes 1–3) and to the decrease in cell growth. Transduction of hTERT transiently and markedly increased the hyperphosphorylated form (Figure 3A, lane 4), corresponding to the sudden recovery in proliferation and to a shorter doubling time. Finally, both hyper- and hypophosphorylated forms of RB remained at steady-state levels (Figure 3A, lanes 5–7), although the hypophosphorylated form seemed dominant at PD 53 (Figure 3A, lane 6), perhaps due to the higher cell density at collection of cell lysate. The protein level of RB was down-regulated in E7-overexpressing UCBE6E7-20 cells (Figure 3A, lane 8), probably as a result of enhanced proteolysis by E7.

Increase in Telomerase Activity and Maintenance of Telomere Length in Cells Transduced with the hTERT

Telomerase activity is revealed by the characteristic six base pair ladder of bands detected by TRAP assay (Figure 4A). No telomerase activity was detected in UCBMSCs at any PDs tested, UCBE6E7-20 cells, UCBMSCs infected with the vector-alone or CHAPS buffer, or mock infected. By contrast, the cells transduced with the hTERT exhibited significant levels of telomerase activity, comparable to HeLa cells as a positive control and to TSR8, which is a synthetic template of eight telomeric repeats used as a polymerase chain reaction (PCR)-positive control.

Average telomere length was longer in the UCBTERT-21 cells than in UCBMSCs. Telomere length in UCBMSCs decreased with the number of PDs, whereas it remained the same in UCBTERT-21 cells, regardless of the number of PDs. The telomere length of UCBE6E7-20 cells was shorter than that of the parental UCBMSCs at senescence.

Normal Diploid Karyotypes with XY Sex Chromosomes in UCBMSCs and UCBTERT-21 Cells

Karyotypic analyses of UCBMSCs were performed at PD 5 (2 passages) and of UCBTERT-21 cells at PD 32 (14 passages). UCBMSCs and UCBTERT-21 cells were found to be diploid and not to exhibit any significant chromosomal abnormalities (Figure 5, A and B). The chromosome number of both UCBMSCs at PD 5 and UCBTERT-21 cells at PD 35 was 46, except for one UCBTERT-21 cell, which contained 47 chromosomes (Figure 5C). No UCBTERT-21 cells containing abnormal numbers of chromosome were found on further analysis. The sex chromosomes were found to be XY, indicating that the cells were of fetal origin.

Osteogenic and Adipogenic Differentiation Potentials of UCBMSCs and UCBTERT-21 Cells

The multipotency of UCBMSCs and UCBTERT-21 cells was assessed by conventional protocols. The osteogenic differentiation potential of UCBMSCs and UCBTERT-21 cells was assessed based on their morphology and von Kossa staining after 3 wk of induction (Figure 6). Multiple small Oil-Red-O–positive fat droplets had accumulated in UCBMSCs and UCBTERT-21 cells after 3 and 2 wk, respectively, of adipogenic induction. Adipocyte differentiation was estimated by counting 2000 cells per dish. The results of triplicate experiments showed that 5.0 and 5.4% of the UCBMSC and UCBTERT-21 cells became positive for fat droplets with Oil-Red stain as a result of adipogenic induction and >90% of the cells were positive on ALP staining after osteogenic induction. We also induced these cells to differentiate into multiple lineages by the methods for neural (Kohyama *et al.*, 2001), cardiomyogenic (Makino *et al.*, 1999; Takeda *et al.*, 2004), and chondrogenic (Imabayashi *et al.*, 2003) lineages; however, the UCBMSC and UCBTERT-21 cells were not induced to differentiate into these lineages in vitro.

DISCUSSION

This study was undertaken to obtain human UCB-derived fetal cells that retain critical cell functions, the same as bone marrow-derived mesenchymal stem cells, mammary gland

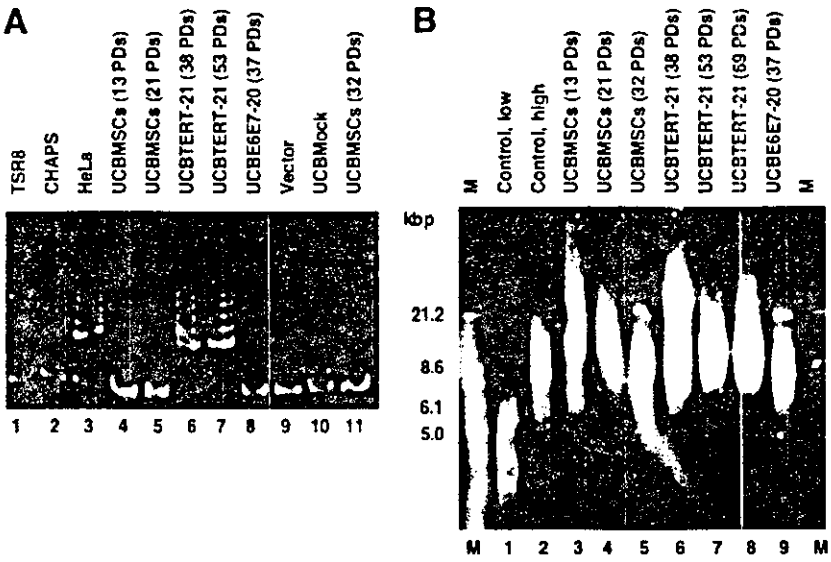

Figure 4. Telomerase activity and telomere length of UCBMSCs, UCBE6E7-20 cells, and UCBTERT-21 cells. (A) Analysis of telomerase activity by the PCR assay in UCBMSCs, UCBE6E7-20 cells, and UCBTERT-21 cells. Telomerase activity is revealed by the characteristic six-base pair ladder of bands. No telomerase activity was detected in the UCBMSCs at PD 13, 21, or 32 (lanes 4, 5, and 11, respectively), the UCBE6E7-20 cells at PD 37 (lane 8), the UCBMSCs infected with the vector alone (lane 9), the CHAPS buffer alone (lane 2) or Mock infected cells (lane 10). By contrast, the UCBTERT-21 cells at PD 38 and 53 exhibited significant telomerase activity (lanes 6 and 7, respectively) that was comparable with that of the HeLa cells (lane 3) and TSR8 (lane 1) as positive controls. (B) Telomere length of UCBMSCs, UCBE6E7-20 cells, and UCBTERT-21 cells. Telomere length was longer in the UCBTERT-21 cells than in the parental UCBMSCs. The telomere length of UCBMSCs at PD 13, 21, and 32 decreased as the number of PDs increased (lanes 3–5). The telomere length of UCBTERT-21 cells was maintained, irrespective of the number of PDs (lanes 6–8). The telomere length of UCBE6E7-20 cells at PD 37 (lane 9) was shorter than that of the parental UCBMSCs at PD 32 (lane 5). Lanes 1 and 2 are control DNAs of short length and long length, respectively.

epithelial cells, skin keratinocytes, and pigmented epithelial cells. It may be possible to use human UCB- and bone marrow-derived stem cells in the future clinically to supply defective enzymes to patients with genetic metabolic diseases, such as neuro-Gaucher disease, Fabry disease, and mucopolysaccharidosis, whose prognosis is poor, and is sometimes lethal. To achieve this, we attempted to prolong the life span of UCB-derived cells or to endow them with immortality without transformation, defining "immortality" simply as indefinite cell division.

Is Successful Prolongation of UCBMSCs Life Span without Inhibition of the p16^{INK4a}/RB Pathway Attributable to a Lack of Ex Vivo Culture Stress?

In contrast to our previous study by using bone marrow-derived cells (Takeda *et al.*, 2004), surprisingly, the successful prolongation of the life span of the UCB-derived fetal cells obtained in this study did not require inhibition of the p16^{INK4a}/RB pathway or premature senescence-associated pathway. Immortalization of some human cell types requires inhibition of the p16^{INK4a}/RB pathway in addition to activation of telomerase (Kiyono *et al.*, 1998; Ishikawa, 2003). Human mammary epithelial cells, endometrial glandular cells, skin keratinocytes, and marrow-derived cells require inhibition of the p16^{INK4a}/RB pathway for immortalization, but foreskin fibroblasts do not. Activation of telomerase alone is sufficient for immortalization of human foreskin fibroblasts. HPV16 E6 and E7 have been used to inhibit p53 and RB, respectively, to prolong the life span of marrow-derived MSCs (Okamoto *et al.*, 2002; Takeda *et al.*, 2004), endometrial gland cells (Kyo *et al.*, 2003), mammary epithelial cells, and keratinocytes (Kiyono *et al.*, 1998). Bmi-1 also has been used to inhibit p16^{INK4a} transcription to prolong the life span of marrow-derived MSCs. One function of this p16INK4a protein is to maintain pRB in a hypophosphorylated active form, which inhibits cell cycle progression.

Our present findings that UCB-derived cells can be immortalized without inhibition of the p16^{INK4a}/RB pathway is consistent with the results in regard to foreskin fibroblasts. This successful immortalization of UCB-cells by hTERT alone can be explained by lack of ex vivo culture stress under the culture condition used in this study. Alternatively, only cells insensitive to ex vivo culture stress or lacking p16^{INK4a} induction may be expanded by hTERT alone. Primary UCB-derived cell culture succeeded in 94% of the attempts (15 of 16 trials), and the cells were passaged only two or three times before reaching premature senescence (13 of 15 primary UCB-derived cell cultures); however, only two cell strains (UCBMSCs) were established from them (2 of 15 primary UCB-derived cell cultures; see *Materials and Methods*. "Isolation and Cell Culture of UCBMSCs"). Based on the results of this study by using one of the two cell strains, the establishment of these strains (UCBMSCs) can be explained by 1) lack of p16^{INK4a} in primary cultured UCB-derived cells or 2) selection of cells that do not express p16^{INK4a} from a heterogeneous population. We cannot exclude either possibilities, and we did observe two different types of cells, i.e., rapidly growing cells and quiescent cells in the primary culture of cord blood cells. If the alternative explanation is true, these quiescent cells, in which p16^{INK4a} may be expressed at a high level, can be efficiently expanded by introduction of E7, the inhibitor of RB, or Bmi-1, the down-regulator of p16^{INK4a}. We also performed additional experiments by using newly obtained specimens from umbilical cord to determine whether infection of the primary or first passage cells generates long-term strains routinely and efficiently. We generated other cells, UCB408 cells, and found that generation of long-term strains was reproducible (Supplementary Figure A). The UCBE6E7-31 and UCBE7-32 cells proliferated for >30 PDs and exhibited persistent growth. The UCBTERT-30 cells exhibited a prolonged cell life span in culture and reached PD 19, but they failed to be immortalized. The success of immortalization of UCBMSCs may still be low, probably due to expression of p16^{INK4a} premature senescence-associated proteins in the early passage of the UCB408 cells. Because the 5′ CpG island of the p16^{INK4a} promoter based on published genome sequences (GenBank accession no. AF022809, U12818, and AC000048) has been found to be methylation-free by the bisulfite method (Supplementary Figures B and C), the lack of

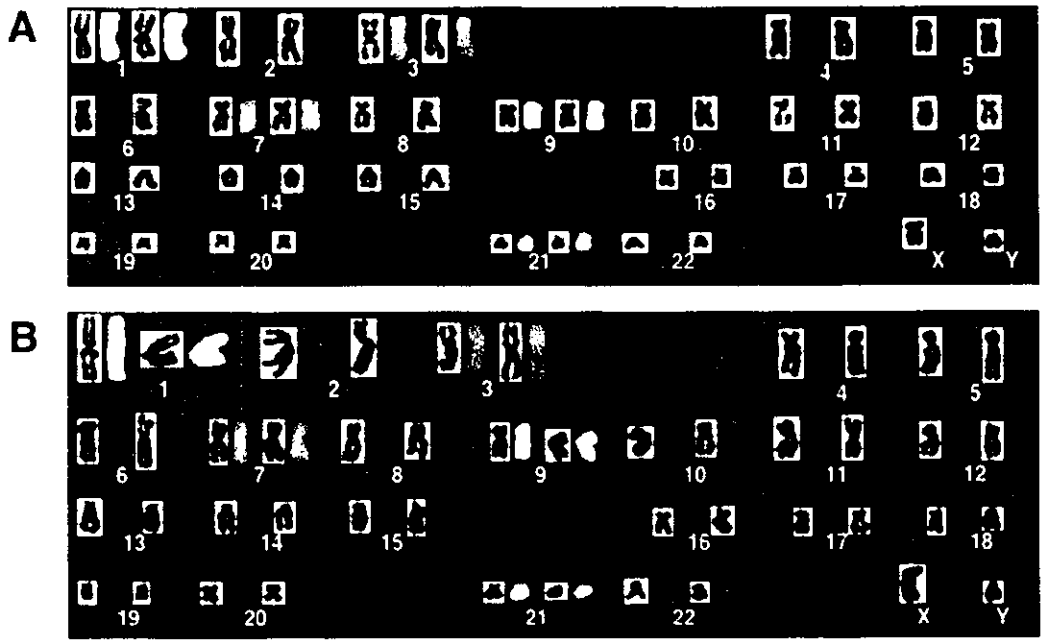

C

Chromosome number		44	45	46	47	48
Number of cells	UCBMSCs, PD5	0	0	50	0	0
	UCBTERT-21, PD35	0	0	49	1	0

Figure 5. Karyotypic analysis of UCBMSCs and UCBTERT-21 cells. Comprehensive karyotyping (left side, reverse DAP, right side, SKY), UCBMSCs at PD 5 (A) and UCBTERT-21 cells at PD 35 (B). Normal diploidy is seen in the UCBMSCs and UCBTERT-21 cells. Both cells were analyzed for chromosome number (C). None of the 50 UCBMSCs tested showed any abnormal numbers of chromosomes. Of the 50 UCBTERT-21 cells tested, 49 exhibited normal diploidy and one cell contained 47 chromosomes. No UCBTERT-21 cells with an abnormal chromosome number were found on further analysis.

$p16^{INK4a}$ expression in rapidly growing cells is not due to methylation of the $p16^{INK4a}$ promoter, unlike human mammary epithelial cells (Umezawa *et al.*, 1997; Foster *et al.*, 1998; Wong *et al.*, 1999).

UCB-derived Cells Are of Mesenchymal Origin

The differentiation capacity of UCB-derived cells was unaffected during establishment of a plate-adhering population of cells from UCB. The cells established from UCB can be extensively and clonally expanded in vitro while retaining their potential to differentiate into osteoblasts that produce mineralized matrices and adipocytes that accumulate lipid vacuoles under in vitro conditions. This differentiation potential of the UCB-derived cells is the same as that reported for bone marrow MSCs (Goodwin *et al.*, 2001; Lee *et al.*, 2004).

The surface markers of the UCB-derived cells examined in this study are exactly the same as those of previously reported UCB-derived cells (Lee *et al.*, 2004). Most of the surface markers are the same as those detected in their bone marrow counterparts (Takeda *et al.*, 2004), with both UCB- and bone marrow-derived cells being positive for CD29, CD44, CD55, and CD59, and negative for CD34 and CD117. The CD90 and CD133 markers, on the other hand, can be used to distinguish UCB-derived cells from bone marrow-derived cells, because they are both expressed in multipotent marrow-derived cells (Takeda *et al.*, 2004) and not in UCB-derived cells (Figure 2) (Lee *et al.*, 2004).

This technique allows the applications of UCB to be further extended and permits it to be used as an alternative to bone marrow as a source of hMSCs; however, this study puts the controversy to rest and substantiates that UCB does contain hMSCs. We believe that the "UCBMSCs" are mesenchymal stem cells derived from UCB, as designated. However, it is difficult to exclude the possibility that the UCBMSCs were derived from mesenchymal cells embedded in the Wharton's jelly of the umbilical cord during insertion of the needle into the vessels through the umbilical cord.

Can primary UCB-derived cell "culture" contribute to cell-based therapy or regenerative medicine? The problems involved in cell-based therapy with human UCB-derived cells are the finite cell life span of the cells and the difficulty of obtaining a large enough number of cells. The technique that allows human cells to escape senescence used in this study may be used to obtain a large number of cells and to overcome these problems of a short life span.

ACKNOWLEDGMENTS

We thank members of Virology Division, National Cancer Center Research Institute (Tokyo, Japan) for helpful discussion and continuous encouragement

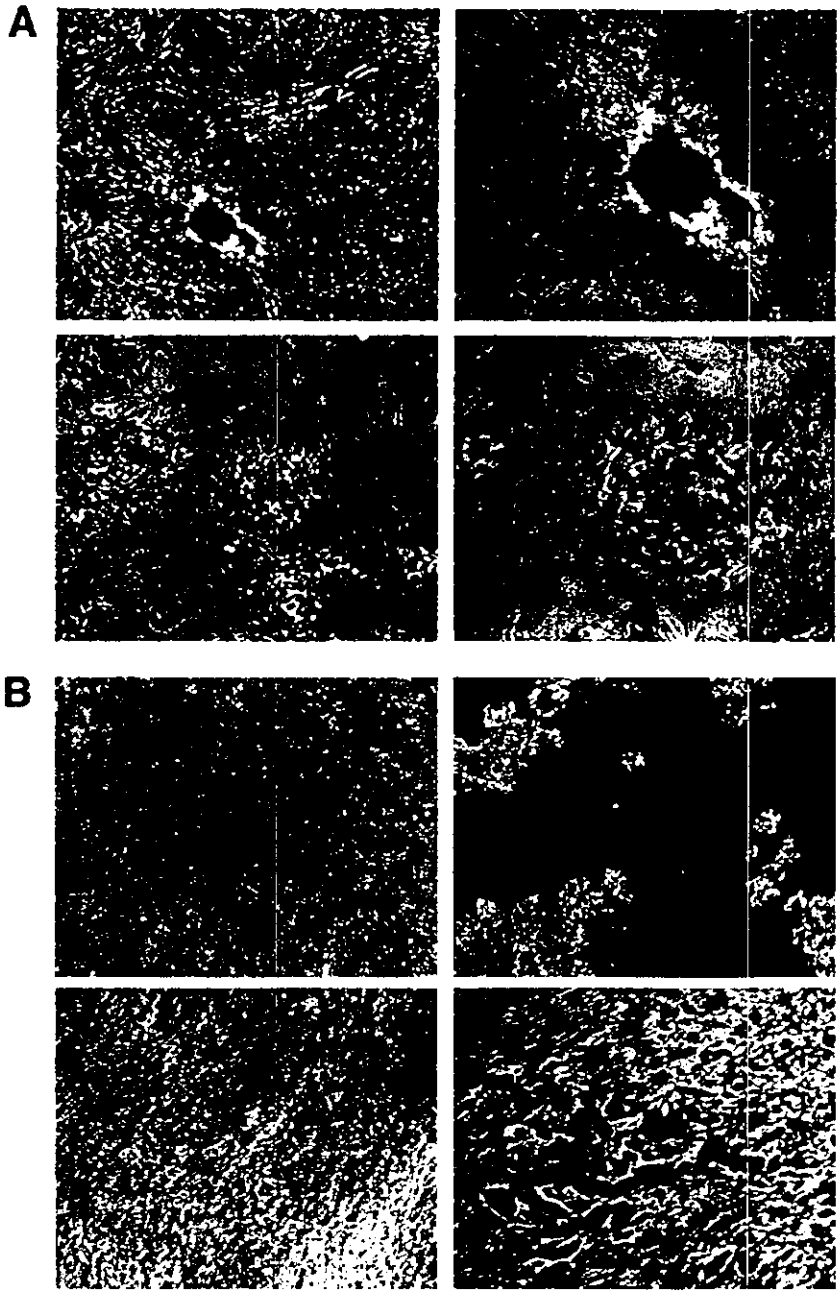

Figure 6. Osteogenic and adipogenic differentiation of UCBMSCs and UCBTERT-21 cells. UCBMSCs (A) and UCBTERT-21 cells (B) were examined by von Kossa staining after 3 wk of osteogenic induction (A and B, top columns) and by Oil-Red-O staining after 2 wk of adipogenic induction (A and B, bottom columns). Both cells contained small lipid vacuoles in their cytoplasm. Original magnifications: (A) left column, 10×; right column, 20×; (B) left column, 5×; right column, 20×.

of this research. This study was supported by a grant from the Ministry of Education, Culture, Sports, Science, and Technology (MEXT) of Japan and the Health and Labor Sciences Research grants (to A. U. and T. K.); the Pharmaceuticals and Medical Devices Agency (to A. U.); an Award for Research Resident Fellowship from the Japan Health Sciences Foundation (to M. T.); and the Japan Association for the Advancement of Medical Equipment (to T. U.).

REFERENCES

Blackburn, E. H. (2000a). Telomere states and cell fates. Nature *408*, 53–56.

Blackburn, E. H. (2000b). Telomeres and telomerase. Keio J. Med. *49*, 59–65.

Blackburn, E. H. (2001). Switching and signaling at the telomere. Cell *106*, 661–673.

Burk, R. D., *et al.* (2003). Distribution of human papillomavirus types 16 and 18 variants in squamous cell carcinomas and adenocarcinomas of the cervix. Cancer Res. *63*, 7215–7220.

Campisi, J. (1997). The biology of replicative senescence. Eur. J. Cancer *33*, 703–709.

Caplan, A. I. (1991). Mesenchymal stem cells. J. Orthop. Res. *9*, 641–650.

Caplan, A. I., and Bruder, S. P. (2001). Mesenchymal stem cells: building blocks for molecular medicine in the 21st century. Trends Mol. Med. *7*, 259–264.

D'Ippolito, G., Schiller, P. C., Ricordi, C., Roos, B. A., and Howard, G. A. (1999). Age-related osteogenic potential of mesenchymal stromal stem cells from human vertebral bone marrow. J. Bone Miner. Res. *14*, 1115–1122.

Dimri, G. P., *et al.* (1995). A. biomarker that identifies senescent human cells in culture and in aging skin in vivo. Proc. Natl. Acad. Sci. USA *92*, 9363–9367.

Foster, S. A., Wong, D. J., Barrett, M. T., and Galloway, D. A. (1998). Inactivation of p16 in human mammary epithelial cells by CpG island methylation. Mol. Cell. Biol. *18*, 1793–1801.

Gewin, L., Myers, H., Kiyono, T., and Galloway, D. A. (2004). Identification of a novel telomerase repressor that interacts with the human papillomavirus type-16 E6/E6-AP complex. Genes Dev. *18*, 2269–2282.

Goodwin, H. S., Bicknese, A. R., Chien, S. N., Bogucki, B. D., Quinn, C. O., and Wall, D. A. (2001). Multilineage differentiation activity by cells isolated from umbilical cord blood: expression of bone, fat, and neural markers. Biol. Blood Marrow Transplant *7*, 581–588.

Hayflick, L. (1976). The cell biology of human aging. N. Engl. J. Med. *295*, 1302–1308.

Imabayashi, H., Mori, T., Gojo, S., Kiyono, T., Sugiyama, T., Irie, R., Isogai, T., Hata, J., Toyama, Y., and Umezawa, A. (2003). Redifferentiation of dedifferentiated chondrocytes and chondrogenesis of human bone marrow stromal cells via chondrosphere formation with expression profiling by large-scale cDNA analysis. Exp. Cell Res. *288*, 35–50.

Ishikawa, F. (2003). Cellular senescence, an unpopular yet trustworthy tumor suppressor mechanism. Cancer Sci. *94*, 944–947.

Jaiswal, N., Haynesworth, S. E., Caplan, A. I., and Bruder, S. P. (1997). Osteogenic differentiation of purified, culture-expanded human mesenchymal stem cells in vitro. J. Cell. Biochem. *64*, 295–312.

Jiang, Y., *et al.* (2002). Pluripotency of mesenchymal stem cells derived from adult marrow. Nature *418*, 41–49.

Kiyono, T., Foster, S. A., Koop, J. I., McDougall, J. K., Galloway, D. A., and Klingelhutz, A. J. (1998). Both Rb/p16^{INK4a} inactivation and telomerase activity are required to immortalize human epithelial cells. Nature *396*, 84–88.

Kohyama, J., Abe, H., Shimazaki, T., Koizumi, A., Nakashima, K., Gojo, S., Taga, T., Okano, H., Hata, J., and Umezawa, A. (2001). Brain from bone: efficient "meta-differentiation" of marrow stroma-derived mature osteoblasts to neurons with Noggin or a demethylating agent. Differentiation *68*, 235–244.

Kyo, S., Nakamura, M., Kiyono, T., Maida, Y., Kanaya, T., Tanaka, M., Yatabe, N., and Inoue, M. (2003). Successful immortalization of endometrial glandular cells with normal structural and functional characteristics. Am. J. Pathol. *163*, 2259–2269.

Lee, O. K., Kuo, T. K., Chen, W. M., Lee, K. D., Hsieh, S. L., and Chen, T. H. (2004). Isolation of multipotent mesenchymal stem cells from umbilical cord blood. Blood *103*, 1669–1675.

Makino, S., *et al.* (1999). Cardiomyocytes can be generated from marrow stromal cells in vitro. J. Clin. Investig. *103*, 697–705.

Mayani, H., and Lansdorp, P. M. (1998). Biology of human umbilical cord blood-derived hematopoietic stem/progenitor cells. Stem Cells *16*, 153–165.

Okamoto, T., Aoyama, T., Nakayama, T., Nakamata, T., Hosaka, T., Nishijo, K., Nakamura, T., Kiyono, T., and Toguchida, J. (2002). Clonal heterogeneity in differentiation potential of immortalized human mesenchymal stem cells. Biochem. Biophys. Res. Commun. *295*, 354–361.

Owen, M. (1988). Marrow stromal stem cells. J. Cell Sci. Suppl. *10*, 63–76.

Pittenger, M. F., Mackay, A. M., Beck, S. C., Jaiswal, R. K., Douglas, R., Mosca, J. D., Moorman, M. A., Simonetti, D. W., Craig, S., and Marshak, D. R. (1999). Multilineage potential of adult human mesenchymal stem cells. Science *284*, 143–147.

Prockop, D. J. (1997). Marrow stromal cells as stem cells for nonhematopoietic tissues. Science *276*, 71–74.

Prockop, D. J., Sekiya, I., and Colter, D. C. (2001). Isolation and characterization of rapidly self-renewing stem cells from cultures of human marrow stromal cells. Cytotherapy *3*, 393–396.

Sasaki, M. S. (1975). A comparison of chromosomal radiosensitivities of somatic cells of mouse and man. Mutat. Res. *29*, 433–448.

Sekiguchi, T., and Hunter, T. (1998). Induction of growth arrest and cell death by overexpression of the cyclin-Cdk inhibitor p21 in hamster BHK21 cells. Oncogene *16*, 369–380.

Sekiguchi, T., Nishimoto, T., and Hunter, T. (1999). Overexpression of D-type cyclins, E2F-1, SV40 large T antigen and HPV16 E7 rescue cell cycle arrest of tsBN462 cells caused by the CCG1/TAF(II)250 mutation. Oncogene *18*, 1797–1806.

Sekiya, I., Larson, B. L., Vuoristo, J. T., Cui, J. G., and Prockop, D. J. (2004). Adipogenic differentiation of human adult stem cells from bone marrow stroma (MSCs). J. Bone Miner. Res. *19*, 256–264.

Takeda, Y., *et al.* (2004). Can the life span of human marrow stromal cells be prolonged by bmi-1, E6, E7, and/or telomerase without affecting cardiomyogenic differentiation? J. Gene Med. *6*, 833–845.

Tsuchiya, K., Mori, T., Chen, G., Ushida, T., Tateishi, T., Matsuno, T., Sakamoto, M., and Umezawa, A. (2004). Custom-shaping system for bone regeneration by seeding marrow stromal cells onto a web-like biodegradable hybrid sheet. Cell Tissue Res. *316*, 141–153.

Umezawa, A., Maruyama, T., Segawa, K., Shadduck, R. K., Waheed, A., and Hata, J. (1992). Multipotent marrow stromal cell line is able to induce hematopoiesis in vivo. J. Cell. Physiol. *151*, 197–205.

Umezawa, A., Yamamoto, H., Rhodes, K., Klemsz, M. J., Maki, R. A., and Oshima, R. G. (1997). Methylation of an ETS site in the intron enhancer of the keratin 18 gene participates in tissue-specific repression. Mol. Cell. Biol. *17*, 4885–4894.

Vaziri, H., Dragowska, W., Allsopp, R. C., Thomas, T. E., Harley, C. B., and Lansdorp, P. M. (1994). Evidence for a mitotic clock in human hematopoietic stem cells: loss of telomeric DNA with age. Proc. Natl. Acad. Sci. USA *91*, 9857–9860.

Wong, D. J., Foster, S. A., Galloway, D. A., and Reid, B. J. (1999). Progressive region-specific de novo methylation of the p16 CpG island in primary human mammary epithelial cell strains during escape from M(0) growth arrest. Mol. Cell. Biol. *19*, 5642–5651.

Cell Tissue Res (2004) 316:141–153
DOI 10.1007/s00441-004-0862-1

REGULAR ARTICLE

Kohei Tsuchiya · Taisuke Mori · Guoping Chen · Takashi Ushida · Tetsuya Tateishi · Takeo Matsuno · Michiie Sakamoto · Akihiro Umezawa

Custom-shaping system for bone regeneration by seeding marrow stromal cells onto a web-like biodegradable hybrid sheet

Received: 28 August 2003 / Accepted: 23 January 2004 / Published online: 4 March 2004

Abstract New bone for the repair or the restoration of the function of traumatized, damaged, or lost bone is a major clinical need, and bone tissue engineering has been heralded as an alternative strategy for regenerating bone. A novel web-like structured biodegradable hybrid sheet has been developed for bone tissue engineering by preparing knitted poly(DL-lactic-*co*-glycolic acid) sheets (PLGA sheets) with collagen microsponges in their openings. The PLGA skeleton facilitates the formation of the hybrid sheets into desired shapes, and the collagen microsponges in the pores of the PLGA sheet promote cell adhesion and uniform cell distribution throughout the sheet. A large number of osteoblasts established from marrow stroma adhere to the scaffolds and generate the desired-shaped bone in combination with these novel sheets. These results indicate that the web-like structured novel sheet shows promise for use as a tool for custom-shaped bone regeneration in basic research on osteogenesis and for the development of therapeutic applications.

Keywords Bone regeneration · Tissue engineering · Scaffold · Marrow stroma · Polymer · KUSA-A1 cells

This work was supported in part by a grant from the Ministry of Education, Culture, Sports, Science, and Technology of Japan, Health and Labour Sciences Research Grants (translational research), and the Organization for Pharmaceutical Safety and Research (to A.U.)

K. Tsuchiya · T. Mori · A. Umezawa (✉)
Department of Reproductive Biology and Pathology,
National Research Institute for Child and Health Development,
Okura, Setagaya, 157-8535 Tokyo, Japan
e-mail: umezawa@1985.jukuin.keio.ac.jp

K. Tsuchiya · T. Mori · M. Sakamoto
Department of Pathology,
Keio University School of Medicine,
160-8582 Tokyo, Japan

K. Tsuchiya · T. Matsuno
Department of Orthopedic Surgery,
Asahikawa Medical College,
078-8802 Hokkaido, Japan

K. Tsuchiya · G. Chen · T. Tateishi
Biomaterials Center,
National Institute for Materials Science,
305-0044 Ibaraki, Japan

G. Chen · T. Ushida
Tissue Engineering Research Center,
National Institute of Advanced Industrial Science and Technology,
661-0974 Hyogo, Japan

T. Ushida
Center for Disease Biology and Integrative Medicine,
School of Medicine, University of Tokyo,
113-0033 Tokyo, Japan

Introduction

New bone for the replacement or restoration of the function of traumatized, damaged, or lost bone is a major clinical and socioeconomic need. Bone formation strategies, although attractive, have yet to yield functional and mechanically competent bone. Autografts (bone obtained from another site in the same subject of the same species) are currently the gold standard for bone repair and substitution, but the use of autografts has several serious disadvantages, such as additional expense and trauma to the patient, the possibility of donor-site morbidity, and limited availability (Glowacki and Mulliken 1985; Bauer and Muschler 2000). Because of these problems, bone tissue engineering has been heralded as an alternative strategy for the regeneration of bone (Langer and Vacanti 1993; Crane et al. 1995; Boyan et al. 1999).

Bone has a highly organized structure composed of a calcified connective tissue matrix formed by the proliferation and differentiation of osteoprogenitors into mature osteoblasts (Maniatopoulos et al. 1988; Pitaru et al. 1993). The osteoblasts belong to the stromal fibroblastic system of the bone marrow, which contains other stromal cells, such as chondrocytes and myoblasts (Friedenstein 1976; Owen and Friedenstein 1988; Haynesworth et al. 1992). We have shown that mouse stromal cells are able to differentiate into cardiomyocytes (Makino et al. 1999;

Gojo et al. 2003), endothelial cells, neuronal cells (Kohyama et al. 2001), and adipocytes (Umezawa et al. 1991). We have previously established a murine osteoblast cell line, KUSA-A1, and shown that clonal stromal cells can generate bone in vivo (Umezawa et al. 1992). Marrow stromal cells are expected to serve as a good source for cell therapy, in addition to embryonic stem cells and fetal cells. Although these precursor cells have been reported to be stem cells, it remains unknown as to whether they are homogeneous or whether they constitute subpopulations of cells committed to various lineages of differentiation (Owen and Friedenstein 1988). The acquisition of a large number of osteoblast precursors as a cell source and the control of differentiation are essential to the success of the production of tissue-engineered bone for clinical application (Minuth et al. 1998).

Temporary three-dimensional scaffolds play an important role in the manipulation of the functions of osteoblasts (Chicurel et al. 1998) and in the guidance of the formation of new bones into the desired shapes (Ishaug et al. 1997; Ishaug-Riley et al. 1998), in the bone tissue-engineering approach. These scaffolds should be biocompatible, osteoconductive, biodegradable, highly porous with a large surface-to-volume ratio, mechanically strong, and malleable into the desired shapes. Synthetic polymers, such as poly(lactic acid), poly(glycolic acid), and poly(DL-lactic-*co*-glycolic acid), which is abbreviated here as PLGA, are easily processed into the desired shapes and are mechanically strong (Langer and Vacanti 1993; Ishaug et al. 1997; Ishaug-Riley et al. 1998; Mikos et al. 1998). Moreover, their degradation time can be manipulated by controlling their crystallinity, molecular weight, and the ratio of lactic acid to glycolic acid copolymer (Thomson et al. 1995). Collagen is the primary component of extracellular bone matrix and has been demonstrated to produce good osteoconductivity (Aronow et al. 1990). Synthetic polymers, on the other hand, lack cell recognition signals, and their hydrophobic properties hinder the uniform seeding of cells in three dimensions. However, since collagen scaffolds are mechanically weak, these materials have been hybridized to combine their advantages and provide excellent three-dimensional porous biomaterials for bone tissue engineering.

We have developed collagen-hybridized PLGA sponge and have reported good biocompatibility both for cartilage tissue engineering with mature bovine chondrocytes (Sato et al. 2001; Chen et al. 2003) and for bone tissue engineering with osteoblasts isolated from marrow cells (Ochi et al. 2003). The sponges organize satisfactory cartilage and bone tissue when the cells fill the pores of the scaffold. The uniform distribution of the cells throughout the scaffolds is imperative for the development of homogeneous tissue, but special seeding techniques, such as stir flask culture or perfusion bioreactor culture, are required to produce an even distribution reliably (Vunjak-Novakovic et al. 1998; Freed et al. 1999). Since simple static seeding methods tend to produce an uneven distribution with large patches of cells on the surface, we have hybridized collagen microsponges with PLGA sheets. The sheets have a collagen fiber network in the openings of the PLGA fiber sheets. The findings that the sheets trap cells, that they can be laminated or rolled to control their shape for tissue engineering, and that they also have the capacity to supply minerals by depositing apatite particulates on the surface of collagen microsponges indicate their great advantages. In this study, we have shown that, when the novel web-like structured sheets are used as a scaffold for bone tissue engineering, an even cell distribution and the control of its shape can be achieved.

Materials and methods

Scaffold fabrication

The hybrid sheet was prepared by allowing collagen microsponges to form in the openings of PLGA knitted sheets as previously described (Chen et al. 2003). Briefly, as shown in Fig. 1A, a knitted Vicryl sheet made of polylactin 910 (a 90:10 co-polymer of glycolic acid and lactic acid) was immersed in a type I bovine collagen acidic solution (pH 3.2, 0.5% by weight, Koken, Tokyo, Japan) and frozen at −80°C for 12 h. It was then freeze-dried under vacuum (0.2 Torr) for 24 h to allow the formation of collagen microsponges. The collagen microsponges were further cross-linked by treatment with glutaraldehyde vapor saturated with a 25% aqueous glutaraldehyde solution at 37°C for 4 h. After the cross-linking, the sponge was treated with a 0.1 M aqueous glycine solution to block unreacted aldehyde groups. After being washed with deionized water and freeze-dried, the collagen-hybridized PLGA (PLGA/COL) sheet was complete. The sheets were sterilized with ethylene oxide for cell culture.

Cell culture

KUSA-A1 cells were cultured as described previously (Umezawa et al. 1992; Kohyama et al. 2001; Ochi et al. 2003).

Cell seeding of a PLGA/COL sheet

A PLGA/COL sheet was placed into a 100-mm culture dish (Falcon) and covered with a silicone rubber framework. A 2-ml volume of KUSA-A1 cell suspension at a density of 5×10^6/ml was dropped onto the PLGA/COL sheet (area: 4 cm^2). After cultivation for 6 h, the sheet was turned over and re-seeded with the same number of cells on the reverse side. For comparison, a KUSA-A1 suspension (1×10^7 cells/ml) was injected into collagen hybrid PLGA sponges, and the injected sponges were incubated at 37°C for more than 30 min. The sponges were then transplanted into the subcutaneous tissue of C3H mice as previously described (Ochi et al. 2003).

Scanning electron microscopy

PLGA sheets and PLGA/COL sheets were examined by scanning electron microscopy (SEM). They were cut into small pieces with scissors and coated with gold by means of a sputter coater (Sanyu Denshi, Tokyo, Japan; gas pressure: 50 mtorr, current: 5 mA, coating time: 180 s). The samples were examined with a JSM-6400Fs scanning electron microscope (JEOL, Tokyo, Japan) operated at a voltage of 3 kV.

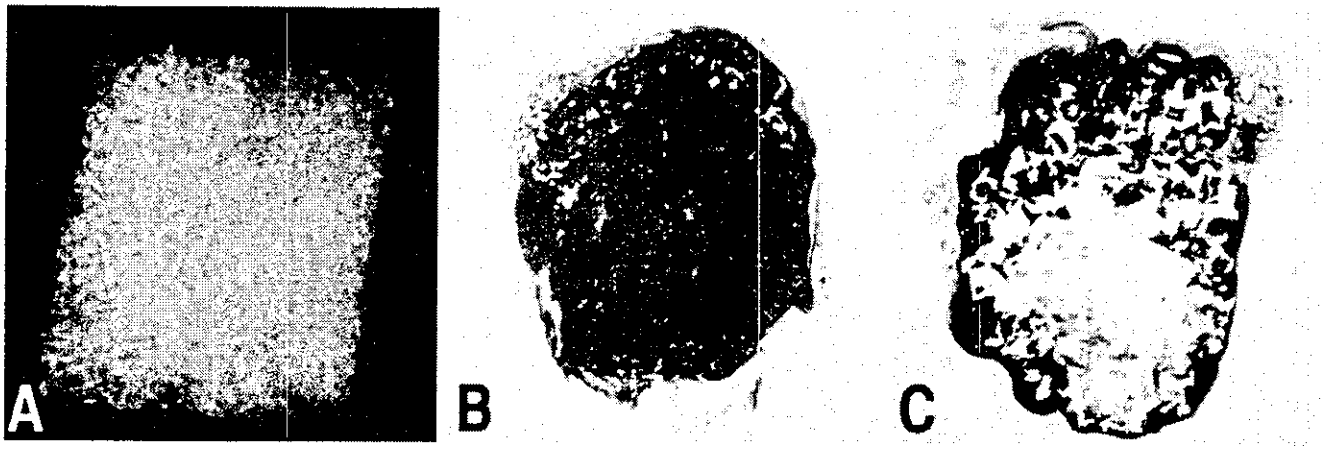

Fig. 1A–C Bone formation in collagen hybrid PLGA sponge. Macroscopic appearance of the collagen hybrid PLGA sponge (**A**). Complete bone formation of an in vivo 4-week construct based on KUSA-A1 cells and collagen hybrid PLGA sponge (**B**). Some constructs showed uneven bone distribution. Living cells did not completely fill the pore cavities of the sponge (**C**). ×5

Transmission electron microscopy

Samples cultured in vitro for 1 day and 2 weeks were examined by transmission electron microscopy (TEM). They were fixed in 2.5% glutaraldehyde, postfixed in 1% osmium tetroxide, dehydrated, and embedded in resin. Ultrathin sections (70–90 nm) were cut and stained with 2% uranyl acetate and Reynold's lead citrate before being examined with a JEM-1200 EX microscope (JOEL) at 80 kV.

In vivo assay

All animals received humane care in compliance with the "Principles of Laboratory Animal Care" formulated by the National Society for Medical Research and the "Guide for the Care and Use of Laboratory Animals" prepared by the Institute of Laboratory Animal Resources and published by the US National Institutes of Health (NIH Publication no. 86–23, revised 1985). The operation protocols were accepted by the Laboratory Animal Care and Use Committee of the National Research Institute for Child and Health Development (Tokyo) and by Keio University School of Medicine.

Laminated sheet implantation onto calvarial defects

Surgery was performed under anesthesia with Nembutal (50 mg/kg, i.p.). A midline skin incision approximately 1 cm long was made on the dorsal surface of the cranium, and the periosteum was removed. A 4.3-mm-diameter full-thickness circular defect was created in the skull with a trephine bar (Hasegawa Medical, Tokyo, Japan) attached to an electric handpiece, with minimal penetration of the dura. The defect was covered with three sheets of cell-loaded scaffolds cut to fit the shape of the defect. The scalp was then closed with 6-0 nylon sutures, and the animals were given access to food and allowed to behave *ad libitum*. Ten defects were left untreated, 10 defects were treated with PLGA/COL sheets alone as controls, and 10 defects were filled with PLGA/COL sheets seeded with KUSA-A1 cells.

Custom-shaped bone formation in mice

With the aim of producing long bone, cylinder-like bone was formed by rolling KUSA-A1-seeded sheets around a silicone rod 3 mm in diameter. The ends of the sheets were hemmed with 4-0 Vicryl dissolvable stitches. The rolled sheets were transplanted into subcutaneous tissue for 4 weeks, flat or after being knotted. Tissue-engineered phalanges were formed in a similar manner. KUSA-A1-seeded sheets were wrapped around a silicone rubber block trimmed in advance to the shape of the distal phalanx and transplanted into subcutaneous tissue. After cultivation in syngeneic C3H/He mice, NOD/SCID mice, and NOD/SCID/IL2-receptor γ knock-out immunodeficient mice (NOG), the specimens were extracted and examined histologically.

Histological and Immunohistochemical staining

Calvaria, femurs, and subcutaneous specimens were dissected at various times after implantation and fixed and decalcified for 1 week in 10% EDTA (pH 8.0) solution. After dehydration in ascending concentrations of ethanol and xylene, the transplants were embedded in paraffin and sectioned. The paraffin sections were then deparaffinized, hydrated, and either were stained with hematoxylin and eosin or were immunohistochemically stained with anti-human Factor VIII mAb (DAKO, Carpenteria, Calif.) to detect angiogenesis.

Results

Bone distribution of sponges

We previously reported that KUSA-A1 cells generated cuboidal bone when used in combination with PLGA/COL hybrid sponge. In those experiments, the KUSA-A1 cells were distributed evenly into sponges and had generated cuboidal bone in the subcutaneous tissue at 8 weeks (Fig. 1A, B); however, some of them exhibited uneven bone formation. The bone was generated mainly at the periphery of the sponge, like an eggshell (Fig. 1C).

Collagen-hybridized PLGA sheet

We developed the sheet-style scaffold to prevent uneven bone formation (Fig. 2A–C). The synthetic biodegradable polymer, PLGA, which was 200 μm thick, was hybridized with collagen microsponges. SEM analysis revealed that the collagen microsponges overlaid the interstices of the

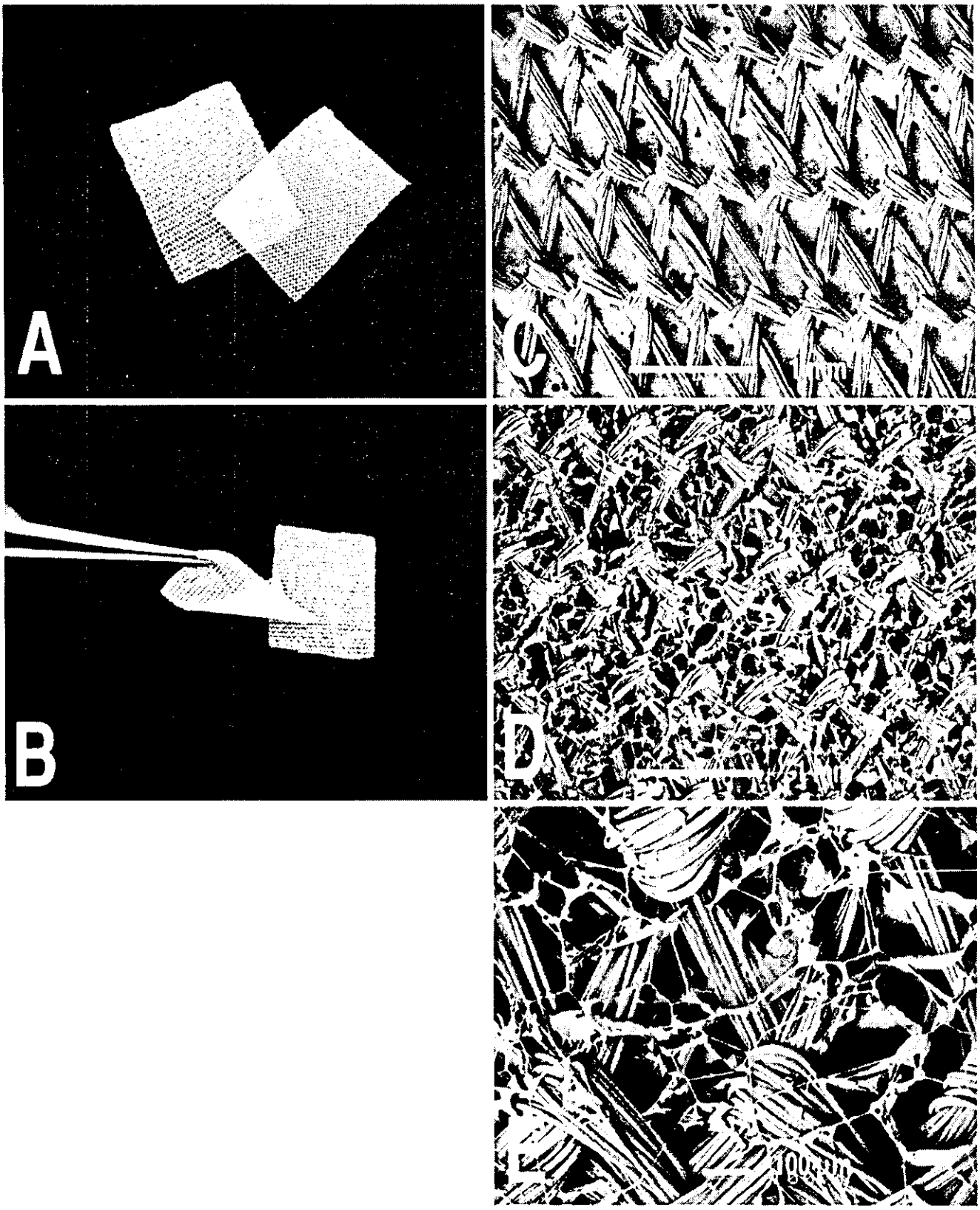

Fig. 2A–E Collagen hybrid PLGA sheet. The thin 200 µm sheets are easy to handle (**A, B**). SEM micrographs of a PLGA sheet without collagen (**C**) and a hybrid sheet with collagen (**D**). Higher magnification of the hybrid sheet (**E**)

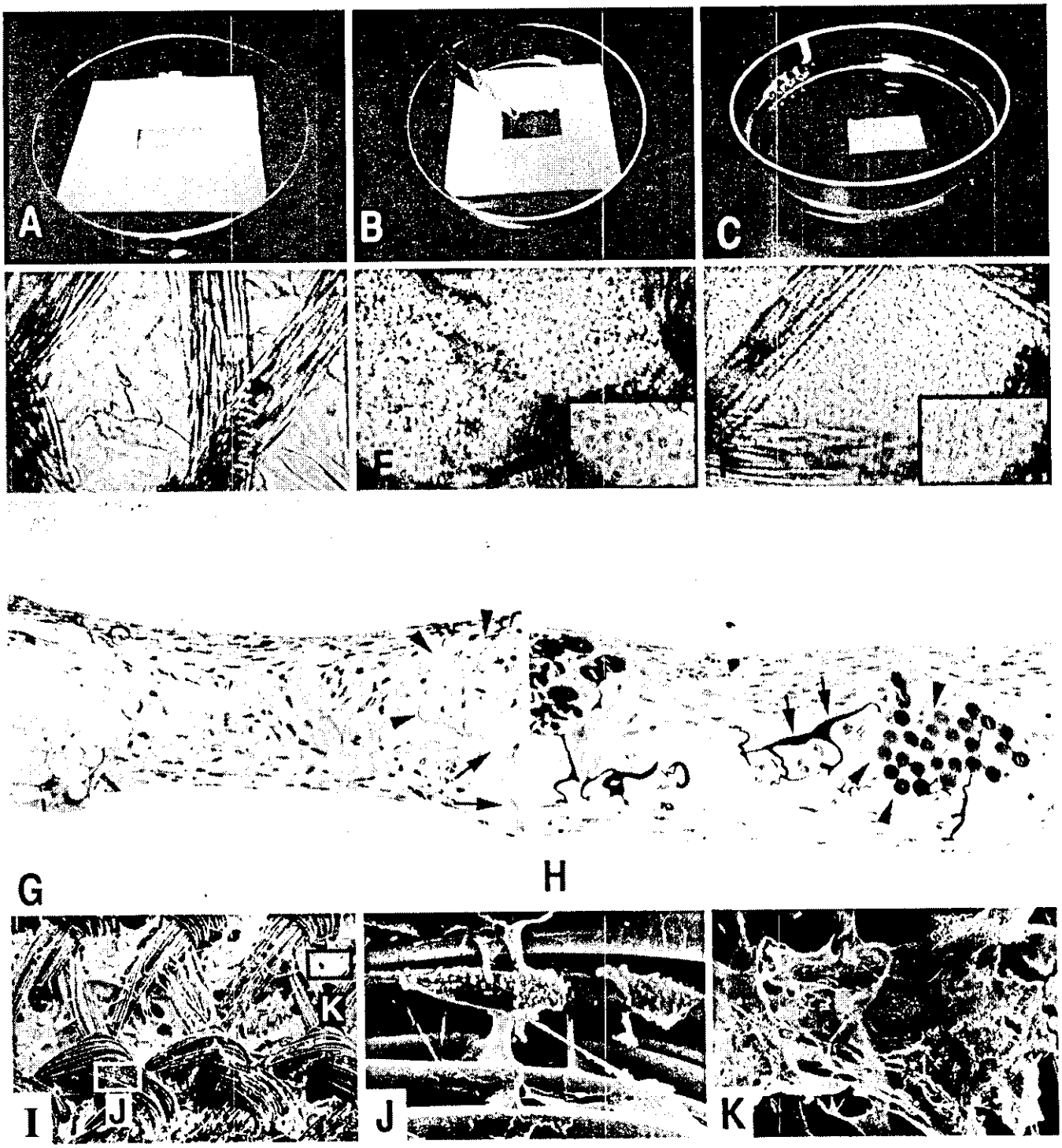

Fig. 3A–K Process of cell seeding. **A–C** Cell seeding of the sheet. The sheet was framed in silicone rubber (**A**), and the cell suspension was simply dropped onto the sheet (**B**). The silicone rubber was removed 6 h after seeding, and the sheet was cultured in growth medium (**C**). **D–F** Phase-contrast micrographs of a cell-seeded sheet. The openings of the PLGA/COL sheet (**D**) were filled with cells at 30 min (**E**) and were completely covered with abundant extracellular matrix at 1 week (**F**). **G, H** Toluidine-blue stained cross sections of the cell-seeded sheet at 1 day (**G**) and 2 weeks (**H**). The thickness of the sheet had increased (*arrowheads* PLGA fibers, *arrows* collagen fibers). **I–K** SEM micrographs of a PLGA/COL sheet after cell seeding. A portion of PLGA fiber (**J**) and collagen microsponge (**K**) are shown. **D–F** ×200, **G, H** ×400, **I** ×50, **J, K** ×200

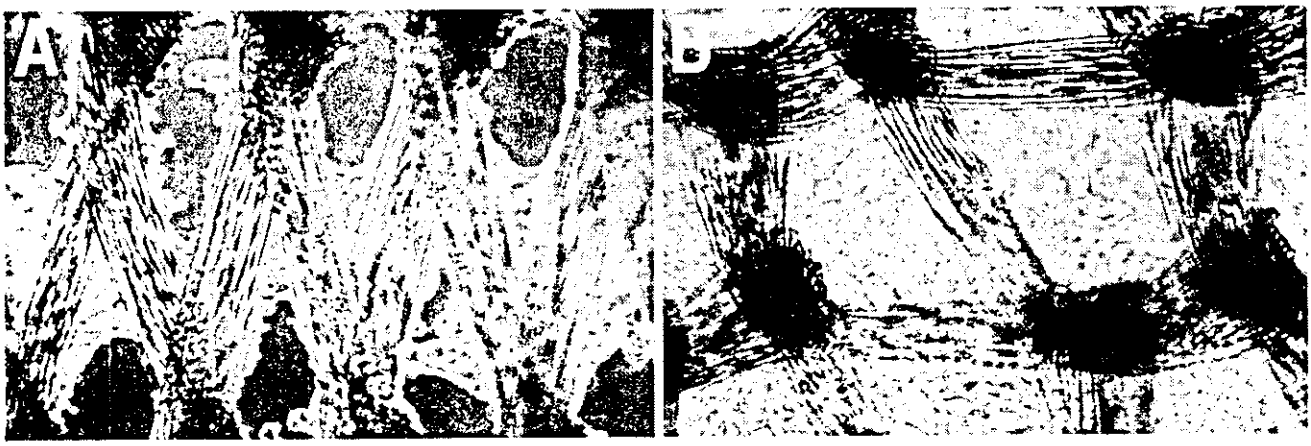

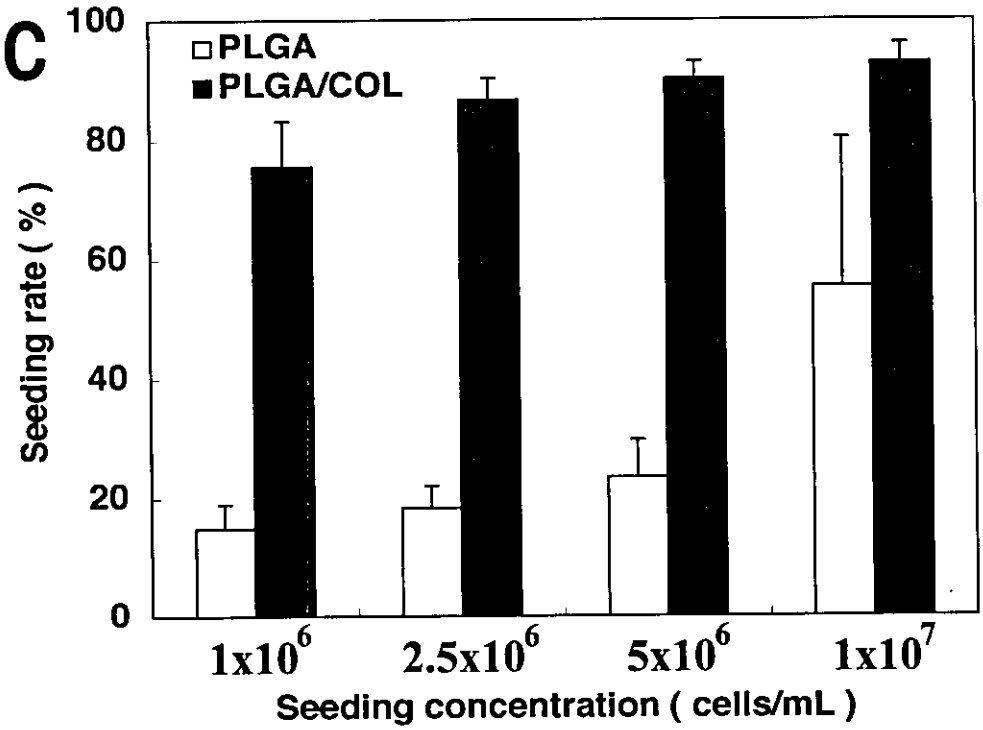

Fig. 4A–C Effect of collagen microsponges on cell adhesion. Microscopic appearance of a PLGA sheet (**A**) and PLGA/COL (**B**) sheet 1 day after seeding the same number of cells in suspension (1×10^7 cells). The seeding rates (**C**) indicate the differences in the number of adhering cells between the two sheets at the initial cell seeding concentrations. **A, B** ×100

fabricated web-like PLGA sheets (Fig. 2D, E). This structure was expected to entrap a large number of cells.

Cells uniformly trapped in sheets with a web-like pattern

A cell suspension was simply dropped onto the sheets (Fig. 3A–C), and the collagen microsponges had filled with precipitated cells 30 min after seeding. The cells had adhered completely at 3 h (Fig. 3D–F), whereas the non-hybridized PLGA sheets did not trap cells efficiently. The cells continued to spread and generate matrix over the sheets, so that at 2 weeks, the sheets were completely covered by extracellular matrix, and the thickness of sheet had increased (Fig. 3G, H). After in vitro culture for 1 day, SEM examination revealed the preference of cells for components of the scaffold (Fig. 3I–K). A large number of cells had adhered to the collagen microsponge portion rather than to the PLGA fibers. Since synthetic polymers lack cell recognition signals, and since their hydrophobic properties hinder cell adhesion, the hybridization of collagen microsponges was advantageous in achieving cell retention.

The PLGA/COL sheets trapped significantly more cells than non-hybridized control PLGA sheets (Fig. 4A, B). The numbers of cells that had adhered to the sheets at 6 h after seeding increased with the initial cell seeding concentration (Fig. 4C).

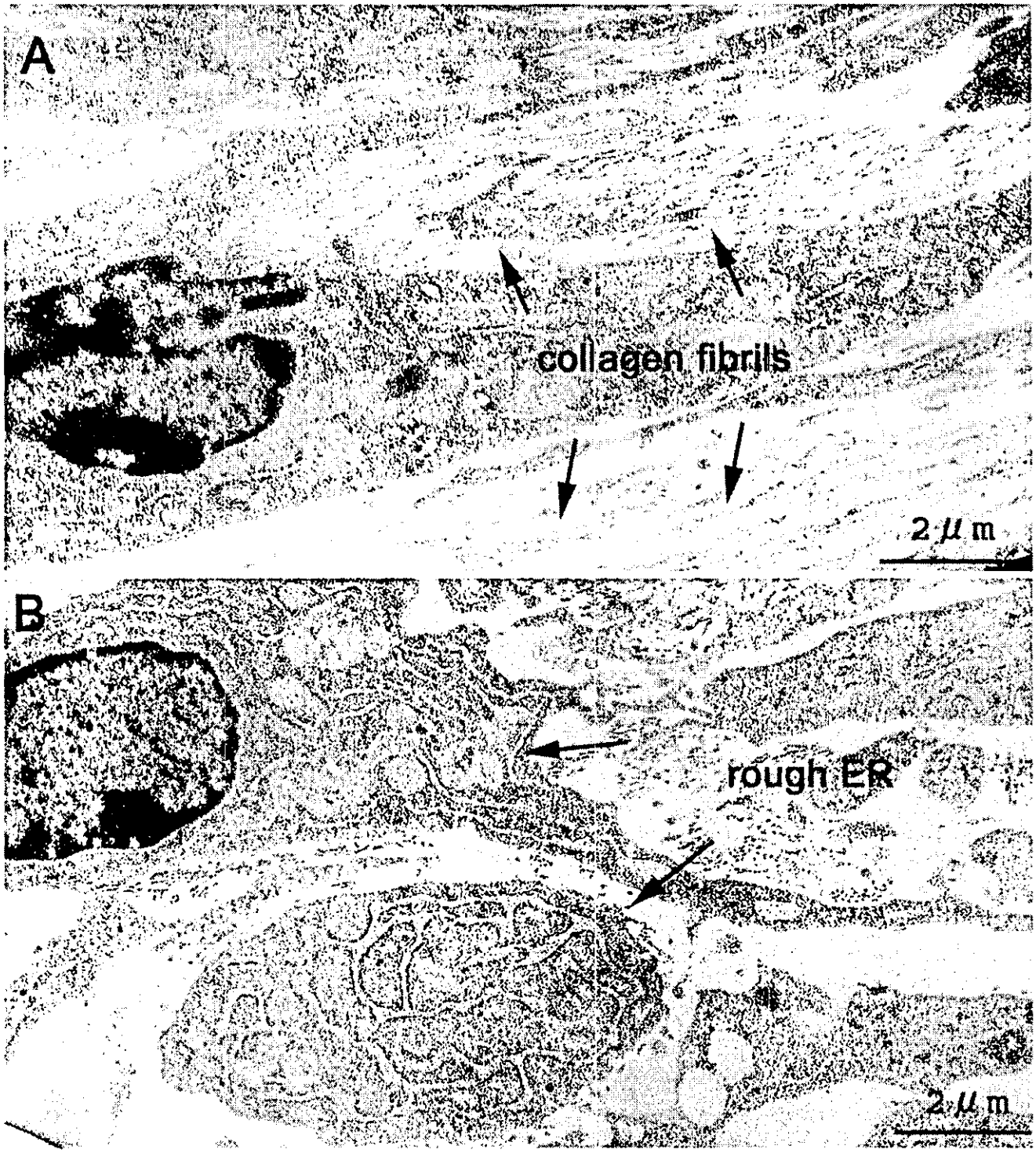

Fig. 5A, B TEM analysis of a PLGA/COL sheet with cells. Ultrastructural analysis was performed 2 weeks after cell seeding. Note the abundant collagen fibrils produced from the cells (**A** *arrows*) and the abundant rough endoplasmic reticulum (*rough ER*) at 2 weeks (**B** *arrows*)

KUSA-A1 cells produce abundant collagen fibrils on the scaffolds

TEM revealed that the cells were tightly adherent to the surface of the PLGA fibers covered with collagen microsponges 24 h after seeding. The cells were spindle-shaped and in close contact to each other. The cell nuclei had become large and bright at 2 weeks, and the nucleoli had also increased in size. The abundant collagen fibrils bridged the intercellular spaces and connected to

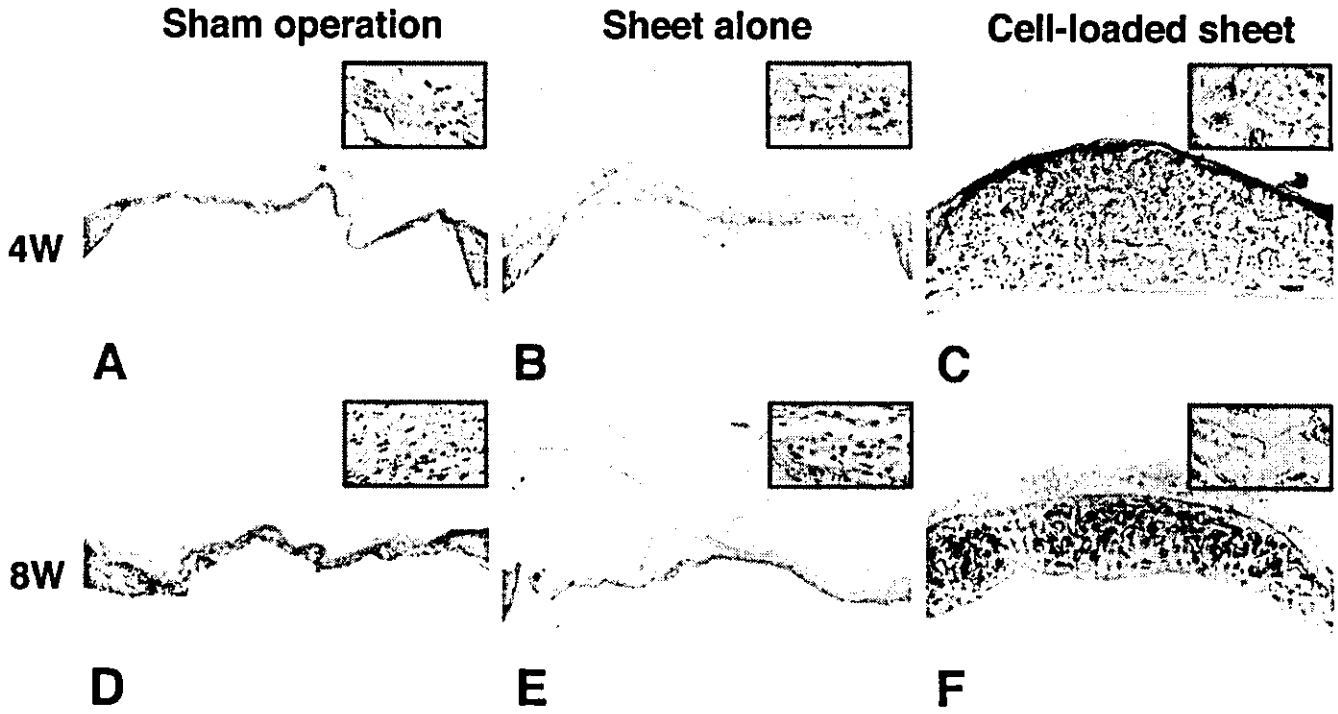

Fig. 6A–F Cranial defects implanted with hybrid sheets containing osteoblasts. No bone formation in the defect is seen at 4 weeks (*4W*) or 8 weeks (*8W*) after a sham operation (**A, D**) or after implantation of PLGA/COL sheets alone (**B, E**). Bone formation can be observed following hematoxylin and eosin staining of KUSA-A1-loaded sheets 4 weeks (**C**) and 8 weeks (**F**) after the sheets were grafted into a cranial defect. *Insets:* High-power views. **A–F** ×20, *Insets* ×200

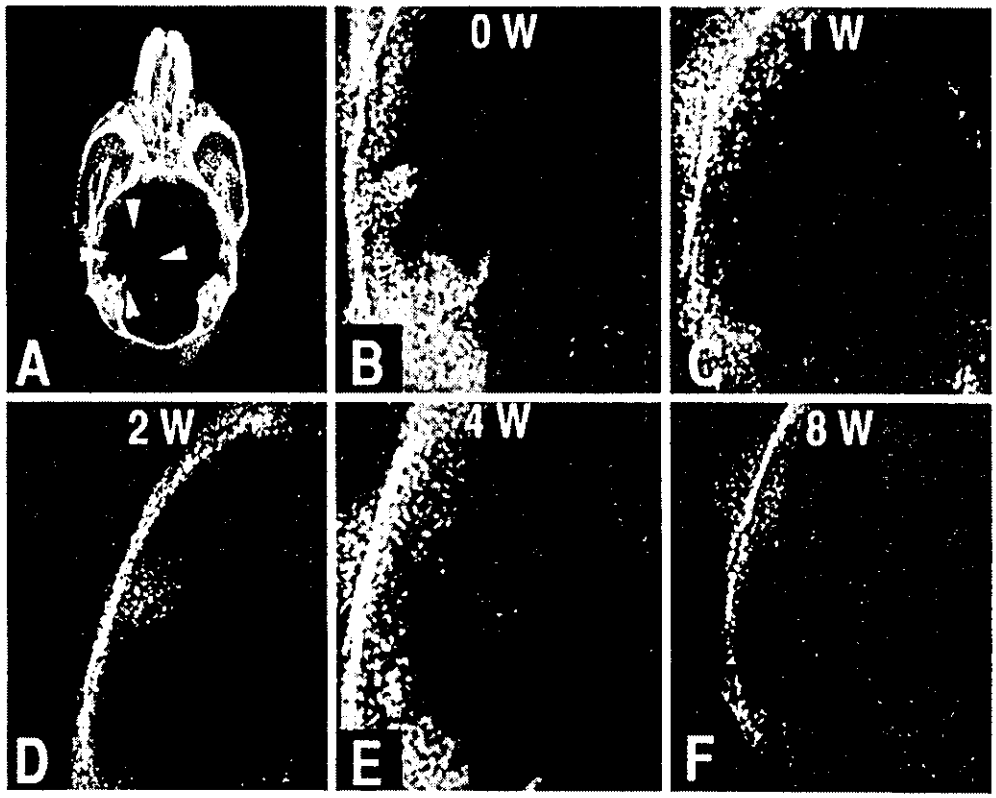

Fig. 7A–F Radiographs of calvaria. **A** A 4.3-mm defect (*arrowheads*) was created on the *left* side of skull. The X-ray density of the KUSA-A1-seeded sheet gradually increased (**B** 0 week, **C** 1 week, **D** 2 weeks, **E** 4 weeks, **F** 8 weeks). **A** ×2, **B–F** ×6